INFORMATION TO USERS

This material was produced from a microfilm copy of the original document. While the most advanced technological means to photograph and reproduce this document have been used, the quality is heavily dependent upon the quality of the original submitted.

The following explanation of techniques is provided to help you understand markings or patterns which may appear on this reproduction.

1. The sign or "target" for pages apparently lacking from the document photographed is "Missing Page(s)". If it was possible to obtain the missing page(s) or section, they are spliced into the film along with adjacent pages. This may have necessitated cutting thru an image and duplicating adjacent pages to insure you complete continuity.

2. When an image on the film is obliterated with a large round black mark, it is an indication that the photographer suspected that the copy may have moved during exposure and thus cause a blurred image. You will find a good image of the page in the adjacent frame.

3. When a map, drawing or chart, etc., was part of the material being photographed the photographer followed a definite method in "sectioning" the material. It is customary to begin photoing at the upper left hand corner of a large sheet and to continue photoing from left to right in equal sections with a small overlap. If necessary, sectioning is continued again — beginning below the first row and continuing on until complete.

4. The majority of users indicate that the textual content is of greatest value, however, a somewhat higher quality reproduction could be made from "photographs" if essential to the understanding of the dissertation. Silver prints of "photographs" may be ordered at additional charge by writing the Order Department, giving the catalog number, title, author and specific pages you wish reproduced.

5. PLEASE NOTE: Some pages may have indistinct print. Filmed as received.

University Microfilms International
300 North Zeeb Road
Ann Arbor, Michigan 48106 USA
St. John's Road, Tyler's Green
High Wycombe, Bucks, England HP10 8HR

INFRA-RED OBSERVATIONS OF INTERSTELLAR MOLECULAR HYDROGEN

by

Thomas Nicholas Gautier III

A Dissertation Submitted to the Faculty of the

DEPARTMENT OF ASTRONOMY

In Partial Fulfillment of the Requirements
For the Degree of

DOCTOR OF PHILOSOPHY

In the Graduate College

THE UNIVERSITY OF ARIZONA

1 9 7 8

THE UNIVERSITY OF ARIZONA

GRADUATE COLLEGE

I hereby recommend that this dissertation prepared under my direction by Thomas N. Gautier III

entitled Infra-red Observations of Interstellar Molecular Hydrogen

be accepted as fulfilling the dissertation requirement of the degree of Doctor of Philosophy

Dissertation Director — Date: Aug. 8, 1978

After inspection of the final copy of the dissertation, the following members of the Final Examination Committee concur in its approval and recommend its acceptance:*

Rodger I. Thompson	Aug 8, 1978
D.A. Shirtina Hall	Aug 8, 1978
R.E. Williams	8 August 1978
Neville J. Woolf	8 Aug '78

*This approval and acceptance is contingent on the candidate's adequate performance and defense of this dissertation at the final oral examination. The inclusion of this sheet bound into the library copy of the dissertation is evidence of satisfactory performance at the final examination.

STATEMENT BY AUTHOR

This dissertation has been submitted in partial fulfillment of requirements for an advanced degree at The University of Arizona and is deposited in the University Library to be made available to borrowers under rules of the Library.

Brief quotations from this dissertation are allowable without special permission, provided that accurate acknowledgment of source is made. Requests for permission for extended quotation from or reproduction of this manuscript in whole or in part may be granted by the head of the major department of the Dean of the Graduate College when in his judgment the proposed use of the material is in the interests of scholarship. In all other instances, however, permission must be obtained from the author.

SIGNED: Thomas N. Bautista III

ACKNOWLEDGMENTS

Like all large projects of this nature this dissertation could not have been completed without the contributions of many fine people. I would like to particularly acknowledge the timely assistance of Dr. Marcia Lebofsky on several occasions during the observational phase of this research, the advice and assistance of Drs. Harold Larson and Uwe Fink and Richard Treffers throughout the project, and the near herculean efforts of my typist, Nancy Moore, to meet the required deadlines. My parents and friends supplied unlimited quantities of much needed moral support and the many members of the University of Arizona's Lunar and Planetary Laboratory are thanked for their always willing scientific and technical support. Financial support came from the National Science Foundation, the National Aeronautics and Space Administration, and was supplemented, in small part, by Nocturnal Aviation. Last, but most important, I want to thank Dr. George Rieke, my advisor, for his support, assistance and patience, without which this dissertation would not have been possible.

TABLE OF CONTENTS

TABLE OF CONTENTS--Continued

LIST OF TABLES

LIST OF ILLUSTRATIONS

LIST OF ILLUSTRATIONS--(Continued)

ABSTRACT

Early in 1976 the present author and associates reported the original detection of infra-red emissions from molecular hydrogen in interstellar molecular clouds. Several lines of the 1-0 quadrupole vibration-rotation band of H_2 were seen in the spectrum of part of the OMC-1 molecular cloud in Orion. Analysis of these emissions revealed the unexpected result that the excited molecular hydrogen appeared to be thermally excited to a temperature near 2000K. Column densities in the neighborhood of 10^9 H_2 molecules cm^{-2} were derived for the observed region. We suggested that heating by interstellar shock waves might be responsible for the observed H_2 emissions. Other authors compared the volume density of molecules needed to thermalize H_2 with our derived column densities to deduce that the observed H_2 probably occurred in thin sheets, compatible with the geometry to be expected from shock heating. An ultra-violet fluorescence mechanism was shown to be an unlikely candidate for the excitation mechanism. Subsequent theoretical work by several groups on shock heating of H_2 has shown that this mechanism can produce the emission spectrum observed from Orion. Problems remain, however, in finding an adequate energy source to drive the required shock in the Orion region. Shortly after the discovery of H_2 emissions from Orion some of the same emission lines were detected by the same group in the spectrum of the planetary nebula NGC 7027.

A decision was made to pursue a general survey for new molecular hydrogen emission sources. The 1-0 S(1) line of H_2 was chosen for the survey because it was expected to be bright under a variety of possible excitation conditions. A wide field, narrow band, tunable monochromator and a matching indium antimonide infra-red detector system were built for particular sensitivity to large, low surface brightness H_2 emission sources. The monochromator used a thin film interference filter as the wavelength selecting element. Tuning was accomplished by tilting the filter with respect to the incoming beam of radiation.

Thirty-three astronomical objects of several types were included in the H_2 survey and four new H_2 sources were discovered. Three of the new sources, Sharpless 140, W3(OH) and NGC 7538 (N)-OH, lie in regions of space similar to the region of the Orion H_2 source and appear to be associated with active star formation. The fourth new source, LkHα 349, lies in a small isolated molecular cloud, not obviously a region of active star formation, and may represent a class of H_2 emission source separate from the H_2 emission sources similar to Orion. Several other types of objects were observed: supernova remnants, dark clouds without imbedded compact IR sources and external galaxies among others. None showed definite signs of H_2 emission to a flux level of about 10^{-12} erg s^{-1} cm^{-2} in a 36" field of view. Other groups have reported detection of 1-0 H_2 emissions in some of these objects at flux levels below those reached in this survey.

The data on the four new sources discovered in this survey are analyzed in terms of current shock heating models and ultra-violet

fluorescence models. Since only the 1-0 S(1) line was observed, no definite distinction could be made between the two excitation mechanisms. The UV fluorescence mechanism is generally unattractive, however, due to the apparent lack of the required sources of ultra-violet flux. The conditions within the new H_2 sources, as determined by the radio molecular observations of other workers, are compatible with the requirements of the shock heating mechanism and, if this mechanism is assumed, the new H_2 emission regions appear to be confined in thin sheets, as was the case with the Orion emission. Possible alternatives to this interpretation are discussed.

CHAPTER 1

INTRODUCTION

Hydrogen is the most abundant element and constitutes roughly 60% of the mass of the universe. Its gravitational attraction controls the dynamics of stellar systems, its nuclear properties dictate the energy generation of most stars and its chemistry dominates the chemistry of all large bodies in the universe. A knowledge of the distribution and physical condition of hydrogen is essential to the understanding of the formation and evolution of stars, the dynamics of galaxies and the physics and chemistry of giant planets (beginning with those in our solar system). At low temperatures the stable form of hydrogen is molecular hydrogen, H_2, and at the low temperatures and high densities encountered in many types of interstellar clouds H_2 is expected to be a sizable fraction of all hydrogen. In very dense clouds ($N(H) \geq 10^3$ cm^{-3}) the formation rate of H_2 on grain surfaces is high enough and the destruction rate low enough that almost all hydrogen will form H_2 on a time scale short compared to the lifetime of the cloud. This would make H_2 extremely important in the dynamics of dense molecular clouds and in the processes of star formation. Unfortunately the inaccessibility of its spectrum has, until recently, made observations of H_2 impossible and has left the great bulk of material in molecular clouds unobservable. This dissertation describes the first

direct detection of molecular hydrogen in a molecular cloud and a subsequent survey for H_2 emission in a wide variety of celestial objects.

The spectrum of molecular hydrogen can best be explained with reference to the energy level diagrams in figures 1 and 2 and the listing in table 1. The only transitions in H_2 of any strength occur either in the vacuum ultra-violet or in the infra-red. In the UV the Lyman and Werner band systems are particularly important since many of them lie below the Lyman continuum for atomic hydrogen and may be excited and observed over long distances in interstellar space. Direct photodissociation is possible with photons shorter than 850A and photoionization with photons shorter than 800A. Radiation associated with these transitions would be masked to a large degree by continuum absorption of atomic hydrogen. Photodissociation can also occur via a permitted transition from the $C^1\Pi_u$ or $B^1\Sigma_u^+$ states to the vibrational continuum of the ground state. A more complete description of the electronic energy levels and the UV spectrum of H_2, as well as a discussion of its astronomical properties is given by Field, Sommerville and Dressler (1966).

In its ground electronic state H_2 has no permanent electric dipole or magnetic dipole moment and the infra-red spectrum of H_2 is produced via electric quadrupole transitions which follow the rotational selection rule $\Delta J = 0, \pm 2$ with $J = 0$ to $J = 0$ forbidden, where J is the rotational quantum number of the states. Several of the important quadrupole transitions within the ground vibrational state, $v = 0$, and between the ground state and the first vibrational state, $v = 1$, are

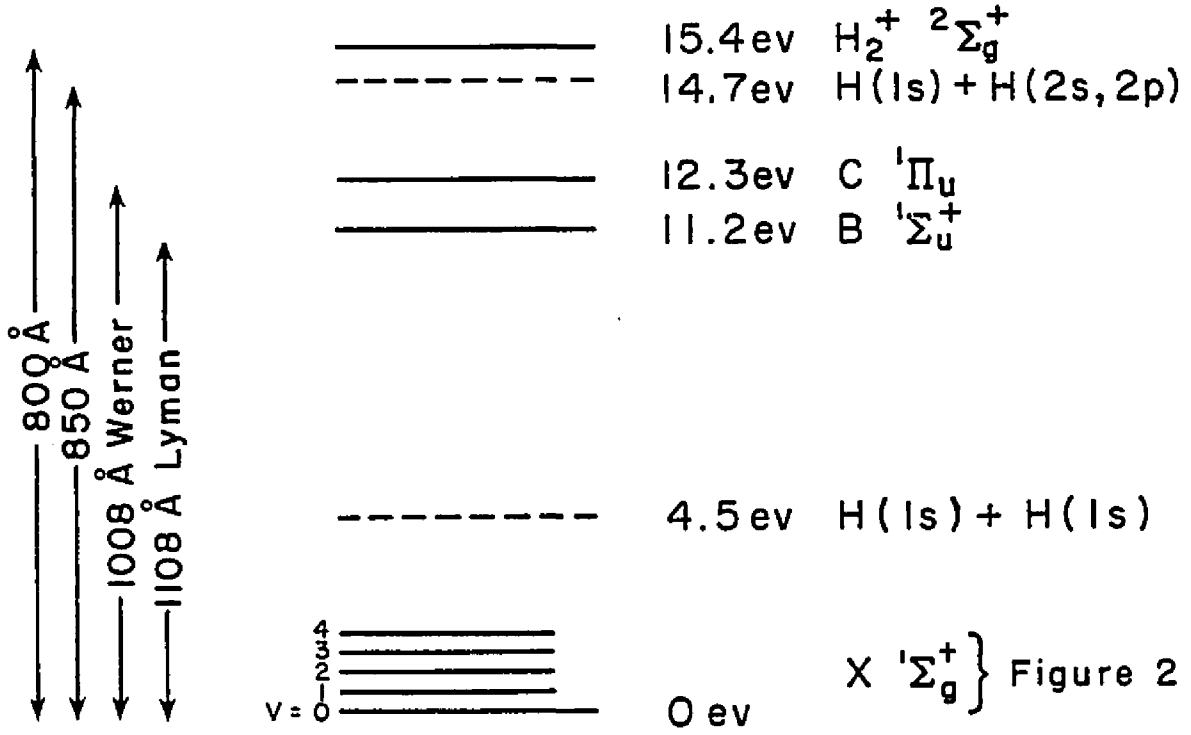

Figure 1. Energy level diagram of molecular hydrogen.

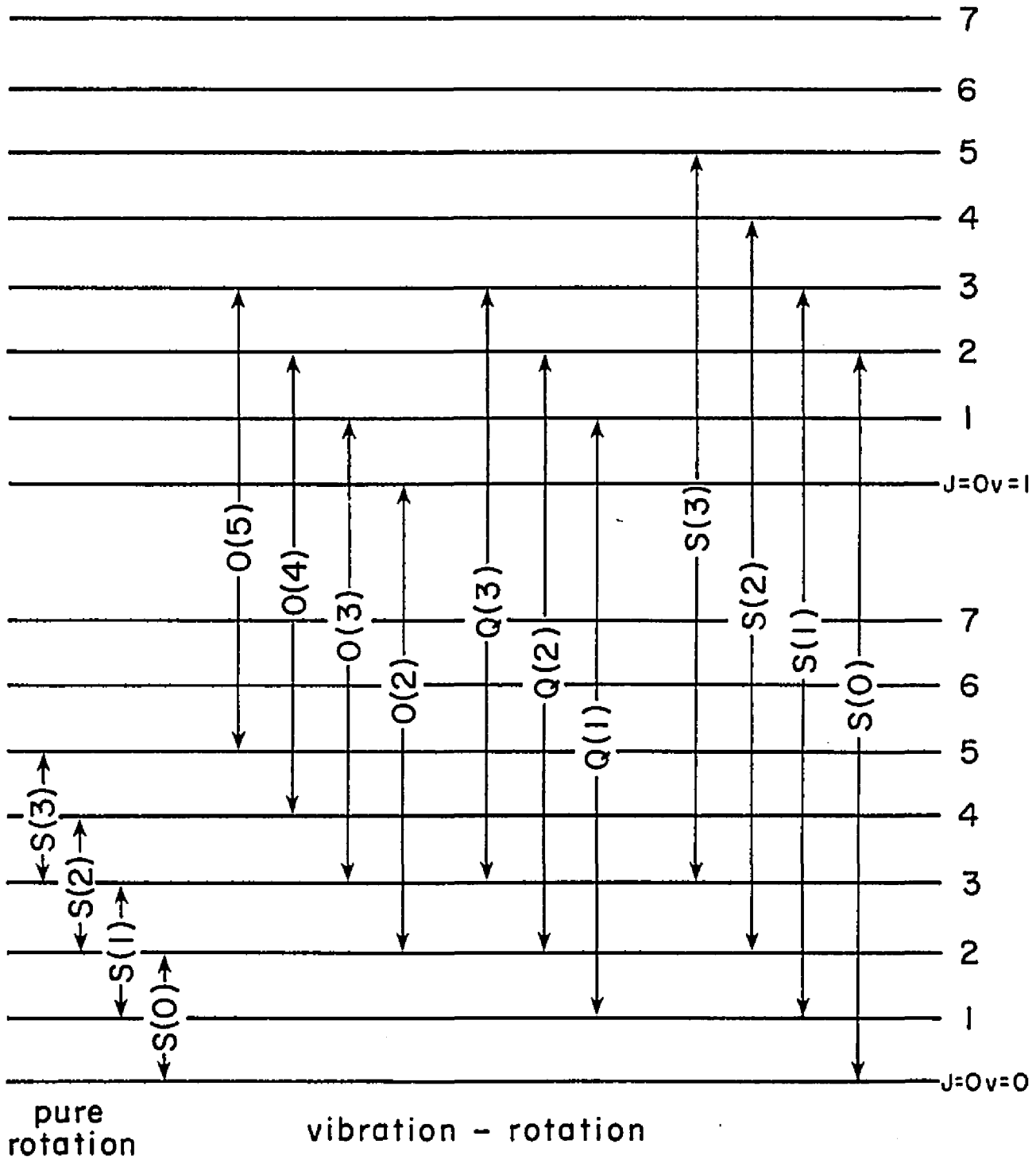

Figure 2. Partial diagram of the lowest vibrational levels of H_2.

Table 1

Ground State Vibration-Rotation Energy Levels in H_2

		Energy (cm^{-1})				
		V				
		0	1	2	3	4
	0	0.00	4161.17	8087.00	11782.4	15252.1
	1	118.49	4273.75	8193.80	11883.4	15347.6
	2	354.38	4497.84	8406.37	12084.6	15538.7
	3	705.52	4831.39	8722.70	12384.0	15825.2
J	4	1168.78	5271.39	9139.87	12778.8	16207.3
	5	1740.15	5813.92	9654.07	13265.4	16684.9
	6	2414.88	6454.35	10260.8	13839.3	17258.0
	7	3187.66	7187.39	10954.8	14495.8	17926.6
	8	4052.80	8007.32	11730.7	15229.6	18690.7

This table was derived with molecular constants of H_2 from Fink (1965).

shown schematically in figure 2. Transitions with $\Delta J = J_{upper} - J_{lower} = -2,0,+2$ are called respectively the O, Q and S branches of a band. An individual transition is referred to by its lower state J value, S(1) for example. A band is referred to by the vibrational quantum numbers of its upper and lower states with the upper state always given first. Figure 2 illustrates the first few lines in each of the O, Q and S branches of the 1-0 band. Other possible vibration-rotation bands are the 2-1, 3-2, etc. with $\Delta v = 1$ and the 2-0, 3-1, 3-0, 4-1, 4-0, etc. with $\Delta v > 1$. The pure rotation spectrum of H_2 divides itself naturally from the vibration-rotation spectrum because it lies in the far infra-red while the vibration-rotation spectrum is confined to the near infra-red (table 2). Being quadrupole transitions, all the infra-red transitions of H_2 have low transition probabilities (10^{-6} to 10^{-7} s^{-1} for vibration-rotation transitions and as low as 10^{-11} s^{-1} for pure rotation transitions) and are therefore difficult to observe.

Rocket borne spectrometers first detected astronomical H_2 absorptions in the vacuum ultra-violet (Carruthers, 1970) and more recently an extensive study of molecular hydrogen in diffuse interstellar clouds has been carried out using the Copernicus satellite (Spitzer et al., 1973). While UV studies of H_2 are useful in the understanding of the general interstellar medium they are unfortunately not suited to the study of dense molecular clouds. UV studies can only observe H_2 on the line of sight to an early type star or other hot object and cannot penetrate to any depth into dense clouds due to scattering and absorption by dust. The great utility of infra-red observations of H_2 lies in

Table 2

Wavelengths of Some IR Transitions of H_2

Pure Rotation

		λ(μ)
	S(0)	28.2
	S(1)	17.0
	S(2)	12.3
	S(3)	9.66
	S(4)	8.03

Vibration-Rotation

		λ(μ)		λ(μ)		λ(μ)
(1-0)	O(4)	3.004	Q(3)	2.425	S(0)	2.224
	O(3)	2.803	Q(2)	2.414	S(1)	2.122
	O(2)	2.627	Q(1)	2.407	S(2)	2.035
(2-1)	S(0)	2.356				
	S(1)	2.248				
(2-0)	S(1)	1.162				
(3-0)	S(1)	0.815				

their ability to penetrate to great depth into dark clouds and in fact to see into the heart of regions of active star formation. It is also no small advantage that infra-red studies, at least of the vibration-rotation spectrum, can be carried out from the earth's surface. The intensities of the lowest J pure rotation lines have been predicted to be strong in dense, collapsing clouds (Gould, 1964; Field et al., 1968), but these lines have yet to be detected. The vibration-rotation lines remained undetected despite considerable effort on the part of several investigators until their detection in the Orion molecular cloud by the present author and associates in 1976.

History of the Vibration-Rotation Lines

The observational history of the near infra-red lines of H_2 in astrophysical contexts (excluding planetary studies in this case) has been mainly marked by failures and pitfalls. Spinrad claimed to have observed some 2-0 transitions ($\lambda \sim 1\ \mu$) in several cool stars including α Ori (Spinrad, 1964 and Spinrad, 1966) but later failed to observe lines of the stronger 1-0 band in high resolution spectra of α Ori obtained by P. and J. Connes (Spinrad and Wing, 1969). Lambert, Brooke and Barnes (1973) have subsequently claimed identification of H_2 1-0 lines in α Her consistent with model atmosphere calculations and have suggested alternative identifications for the "2-0 lines" observed by Spinrad. Hall has also observed 1-0 lines in several cool stars (Hall, Hinkle, Ridgway and Wojslaw (unpublished paper).

Osterbrock (1962) pointed out that vibration-rotation emission could be produced in the neighborhood of hot stars by absorption of a

UV photon into an excited electronic state of H_2 followed by decay to excited levels of the ground electronic state. Gould and Harwit (1963) estimated the flux to be expected from this fluorescence process in the 1-0 and 2-0 bands of H_2. No immediate effort was made to observe these lines although Gould and Harwit felt that the emission intensity would be within the capabilities of existing instrumentation. Werner (1968) determined that the fluorescence lines in the 3-0 band near .8 μ should be detectable from HI regions near hot stars with available equipment. Werner and Harwit (1968) then used a pressure scanned fabry-perot interferometer and a photomultiplier detector to search for selected 3-0 lines in several astronomical sources. They reported the detection of the O(2) line in a dark region of the Orion nebula (NGC 1976). A repetition of the O(2) observations with a new fabry-perot by Gull and Harwit (1971) unfortunately failed to confirm the earlier detection.

Some years later Black and Dalgarno (1976) published a detailed calculation of the intensities to be expected from the brightest $\Delta v = 1$, 2 and 3 lines of H_2 excited by UV radiation from nearby hot stars and again indicated that the predicted flux levels were within the capabilities of existing instrumentation. About the same time Gautier, Fink, Treffers and Larson (1976) identified seven lines of the 1-0 band of H_2 in spectra of the Becklin-Neugebauer object and the Kleinmann-Low nebula in the Orion molecular cloud. Aside from the unmistakable existence and identification of these lines the striking conclusion of these observations was that the observed H_2 was not excited by ultra-violet absorption but rather by some process which

produced a thermal population distribution with a temperature of about 2000K. Almost immediately several 1-0 lines were identified in the spectrum of the planetary nebula NGC 7027 by the same group (Treffers, Fink, Larson and Gautier, 1976) and the presence of the Orion emission was confirmed and the emission region mapped by Joyce and Grasdalen (1976). Subsequently, 2 μ H_2 emission has been detected in five more planetary nebulae (Beckwith, Persson and Gatley, 1978), T Tauri (Beckwith, Gatley, Matthews and Neugebauer, 1978), in four more molecular clouds near HII regions (this dissertation) and in the Seyfert galaxy NGC 1068 (Thompson, Lebofsky and Rieke, 1978). Considerably detailed observations of the Orion H_2 emission have also been made by Beckwith, Persson, Neugebauer and Becklin (1978), by Joyce, Gezari, et al. (1978) and by Ogden et al. (unpublished paper).

Outline of Dissertation

After the initial detection of the 2 μ lines in Orion and NGC 7027 the dissertation project which has resulted in this paper was begun. Dr. Rieke suggested that a search for 1-0 H_2 emission with a sensitive, wide field instrument would be a more timely dissertation than the project which had produced the first H_2 spectra from Orion. This suggestion was implemented with the design and construction of a wide field monochrometer and an extensive program of survey observations. The body of this dissertation will detail the instrumentation, observations and results of the H_2 survey beginning with a description of the original Orion detection. Considerable effort was put into the survey instrument and an entire chpater is devoted to its description. A

quick treatment of the recent theoretical results concerning shock heating of H_2 is given as background for the interpretation of the survey results. The survey is then described and the results presented. Lastly the survey results are analyzed in terms of current theoretical models of molecular hydrogen excitation.

CHAPTER 2

INITIAL DETECTION OF THE 1-0 LINES

The 2 μ emission from H_2 was originally discovered somewhat by accident in the course of a research project into the nature of compact infra-red sources undertaken by myself. As reported in Gautier et al. (1976), I, Richard Treffers, Harold Larson and Uwe Fink had used the Steward Observatory 229 cm (90 in.) telescope and the Lunar and Planetary Laboratory's fourier transform spectrometer to obtain a low resolution 2 μ spectrum of the Becklin-Neugebauer object in the Orion nebula on 23 October 1975. This spectrum showed an unidentified line at 2.12 μ. To confirm the existence of this line and to obtain a more accurate wavelength measurement we used the 229 cm telescope again on 15, 16 January 1976 to produce higher resolution (3.3 cm^{-1}, $\nu/\Delta\nu$ = 1500 at 2 μ) spectra of BN and the nearby Kleinmann-Low Nebula. These new spectra confirmed the presence of the 2.12 μ line and showed several new unidentified emission features as well. Treffers subsequently identified the 2.12 μ line as the 1-0 S(1) line of molecular hydrogen and we found six more 1-0 lines among the newer unidentified emissions.

Observations

The fourier transform spectrometer used was a rapid scanning type with a resolution capability of 0.5 cm^{-1} and is described more fully by Larson and Fink (1975). Dual input beams were used for sky

cancellation and a liquid nitrogen cooled indium antimonide detector was used in each of the two output beams. Cooled filters restricted the spectral passband to 0.83 - 2.7 μ. The maximum path difference in the interferograms was 0.18 cm, producing spectra with an unapodized resolution of 3.29 cm^{-1}. The detector's field of view was 7.3" square (1.25×10^{-9} sr), and the separation between the input beams was 84". Spectra were taken both of BN and part of the Kleinmann-Low nebula 10" south of BN. These spectra along with the spectrum of a comparison star (η Boo, GOIV) and a ratio spectrum of BN are displayed in figures 3 and 4. The spectrum of η Boo indicates the positions of interfering telluric H_2O (>5000 cm^{-1} and <4200 cm^{-1}) and CO_2 (4850 cm^{-1} and 4974 cm^{-1}) absorptions. The ratio spectrum of BN was produced by dividing the spectrum of BN by the η Boo spectrum and multiplying the result by the calculated spectrum of a 5920K blackbody, appropriate to the effective temperature of a GOIV star. The spectrum of BN represents about 2.1 hours of effective integration time; that of KL, about 0.3 hours.

The locations of the input beams are shown in figure 5 as diamonds representing the actual projections of the detector on the sky. The spectrum of BN in figure 3 is the average of two spectra, one taken with the signal beam at A and the reference beam at A' and one taken with the signal beam at A and the reference at A". B and B' represent the signal and reference beam positions respectively for the spectrum of KL shown in figure 4.

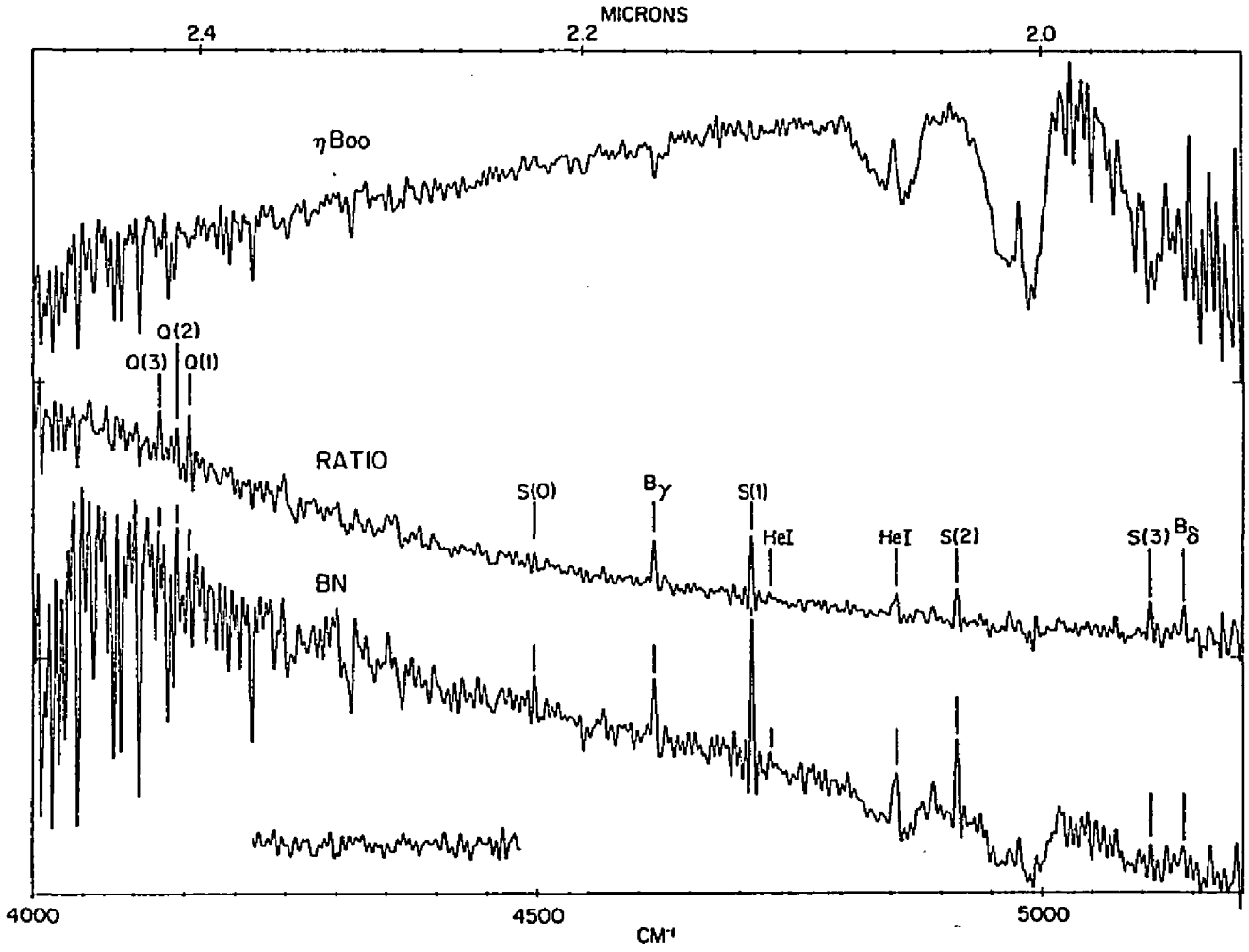

Figure 3. Spectrum of the Becklin-Neugebauer object. -- 3.29 cm^{-1} resolution with a 7.3" square field of view. H_2 emission lines are marked. A sample of noise from a region of zero signal in the BN spectrum is shown.

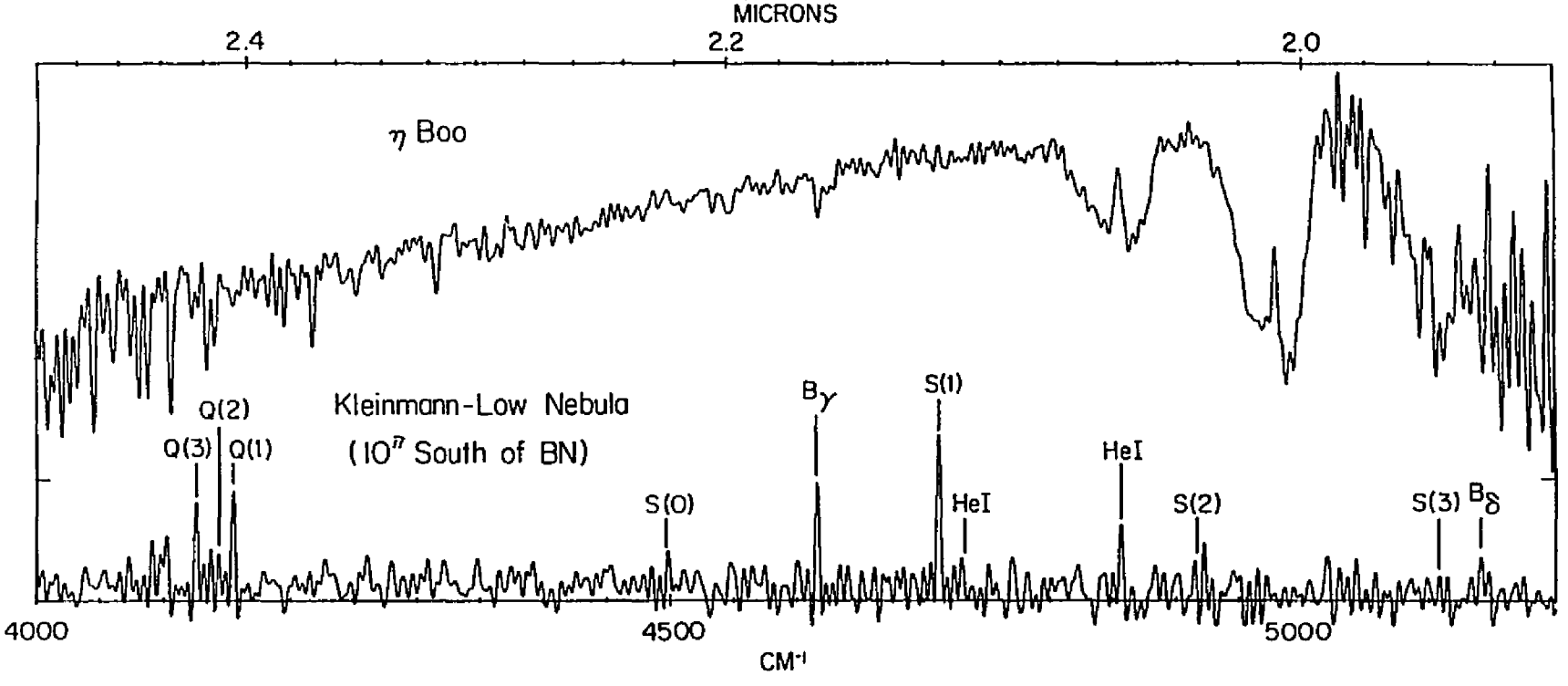

Figure 4. Spectrum of a region 10" south of BN in the Kleinmann-Low Nebula. -- The resolution is 3.29 cm^{-1} and the field of view was 7."3 square.

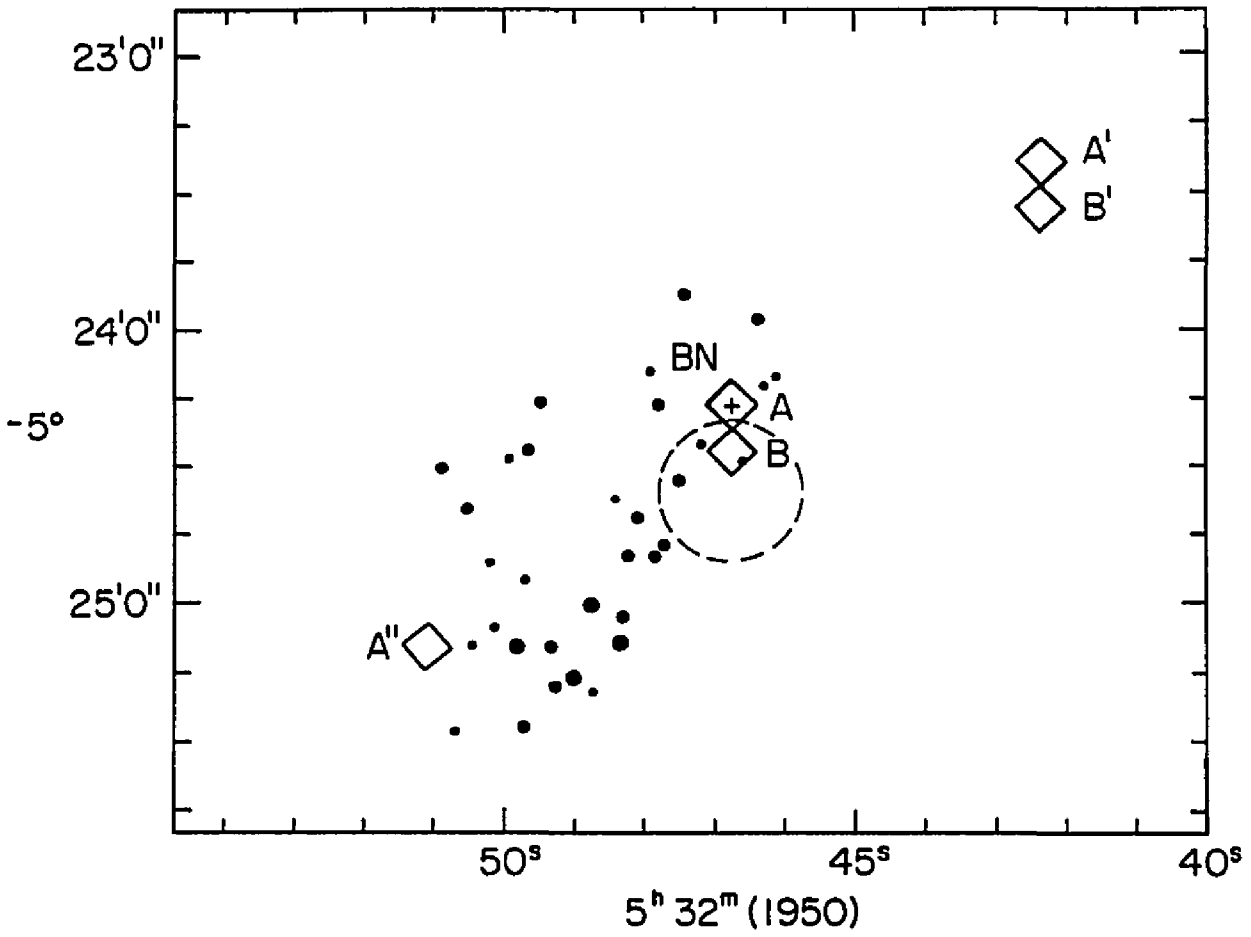

Figure 5. Schematic representation of the location of the spectrometer entrance apertures. -- The dotted circle shows the approximate location of the Kleinmann-Low Nebula. The cross gives the position of the Becklin-Neugebauer object. Diamond shaped Figures A and B give the size and location of the signal beams. A', A'', and B' represent the reference beams. Map adapted from Becklin and Neugebauer (1968).

Identification and Flux Calibration

Table 3 gives the positions of seven lines of the H_2 1-0 quadrupole vibration-rotation spectrum which are visible in our spectra. None of the seven are wider than our instrumental profile. With the exceptions of S(0) and S(2) in KL, which are badly distorted by noise, all H_2 lines indicated fall within 1 cm^{-1} of their laboratory positions. Heliocentric radial velocities derived from the strong S(1), Q(1), and Q(3) lines are 10 ± 8 km s^{-1} for BN and 22 ± 8 km s^{-1} for KL. Reduced to the local standard of rest (assuming V_{sun} = 20 km s^{-1}), these become -7 ± 8 km s^{-1} and +5 ± 8 km s^{-1} for BN and KL respectively, consistent with other LSR velocities for Orion of ∿-3 km s^{-1} for HII recombination lines and ∿+9 km s^{-1} for radio molecular emission (Liszt et al., 1974).

The absolute fluxes of the H_2 lines in the BN spectrum were calibrated using the continuum level of BN at 2.2 μ and a broad-band 2.2 μ flux measurement taken from Gillett and Forrest (1973). No H_2 flux was assumed to enter the reference beam. Instrumental and atmospheric corrections were determined from observations of the stars η Boo (GOIV) and λ Ser (GOV) as described in Treffers et al. (1976). Since low resolution instrumental corrections cannot properly be applied to emission lines between unresolved telluric absorption features, a higher resolution (0.1 cm^{-1}) spectrum of the Sun was examined to determine the relative positions of telluric lines and H_2 emission lines. Depending on the exact location of the H_2 line, a maximum of 20% telluric absorption is possible, with the exception of S(3) which

Table 3

OBSERVED 1-0 H_2 LINES AND COMPARISON WITH CALCULATED INTENSITIES

Surface brightness normalized to S(1). Absolute value for S(1) and derived column densities are given at bottom.

Line	Rest Frequency* (cm^{-1})	Transition Probability* (10^{-7} sec^{-1})	Measured Frequency (cm^{-1})		Measured Surface Brightness†††		Calculated Surface Brightness		
			BN	KL	BN	KL	2000K	1000K	300K
Q(3)	4125.87	2.29	4125.9	4125.7	0.50±0.12	0.67±0.08	0.54	0.54	0.54
Q(2)	4143.47	2.66	4143.0	4143.2	0.29±0.15	0.14±0.08	0.19	0.25	0.75
Q(1)	4155.26	3.32	4155.0	4154.9	0.61±0.15	0.69±0.08	0.81	1.21	7.86
S(0)	4497.84	2.47	4497.5	4498.9	0.1 ±0.08	0.2 ±0.1	0.20	0.25	0.76
S(1)	4712.91	3.66	4712.7	4712.5	1.0	1.0	1.0	1.0	1.0
S(2)	4917.01	4.48	4916.2	4915.2	0.50±0.08	0.1 ±0.05	0.40	0.29	0.07
S(3)	5108.41	4.27	5107.7		>0.5**		0.98	0.48	0.02
S(1) Absolute surface brightness† (erg $cm^{-2}sec^{-1}sterad^{-1}$)					$3.0\pm0.5\times10^{-3}$	$3.6\pm1\times10^{-3}$††			
Column density around BN (cm^{-2}) based on S(1)							$9.4\pm1.5\times10^{18}$	$1.4\pm0.2\times10^{20}$	$5.0\pm0.8\times10^{26}$

* From laboratory frequency and intensity measurements by Fink, Wiggins, and Rank (1965)

** Strong interference by telluric water

† Using a detector field of view of 1.25×10^{-9} sterad, and a flux from BN of 3.4×10^{-16} w cm^{-2} μ^{-1} at 2.2 μ from a broadband measurement in Gillett and Forrest (1973)

†† Using $S(1)_{KL} = 1.2 \times S(1)_{BN}$ as discussed in text

††† Uncorrected for reddening

may be severely attenuated. Since KL has no observed continuum, a comparison of signal-to-noise ratios between BN and KL was used to determine that the S(1) flux from KL is probably 1.2 ± 0.3 times that from BN. These absolute fluxes are given in table 3. Comparison of individual spectra before averaging indicated that the region A' (84" northwest of BN) may have 15 percent of the H_2 emission strength of BN.

Temperature Analysis

The presence of the excited H_2 in Orion of course raised the question of possible excitation mechanisms. Black and Dalgarno (1976) had published detailed calculations for the expected intensities of 1-0 lines due to excitation by ultra-violet radiation. However, these predicted intensities did not agree with out observed intensities. Black and Dalgarno predicted strong lines from overtone bands (2-1, 3-2, etc.) which we did not observe. Further, their predicted intensity ratios among the lines we did observe did not match the real intensities. As an alternative we attempted to fit an ordinary thermal excitation model to our data. Uwe Fink undertook the calculations for this fitting procedure and an explanation of his method and results follows.

If the observed H_2 lines are optically thin and the molecular energy levels exhibit a Boltzman distribution (collisional excitation is the simplest way to produce this) the observed line intensity for a transition from an upper state 2 to a lower state 1 is given by

$$I_{12} = \frac{N(2J_2 + 1)g_2 h\nu_{21} A_{21}}{Q_v(T)Q_r(T)4\pi} \exp(-(E_{v2} + E_{r2})/kT) \qquad (1)$$

where N is the number of molecules per cm^{-2}, $2J_2 + 1$ and g_2 the angular momentum statistical weight and nuclear spin statistical weight respectively of the upper level, $Q_v(T)$ and $Q_r(T)$ the vibrational and rotational partition functions respectively, $E_{v2} + E_{r2}$ the energy due to rotation and vibration in the upper level, $h\nu_{21}$ the transition energy and A_{21} the spontaneous emission probability in s^{-1}.

Rearranging equation (1) and taking its logarithm results in

$$\ln\left[\frac{4\pi I_{21}}{(2J_2 + 1)g_2 h\nu_{21}A_{21}}\right] - \ln\left[\frac{Q_v(T) + Q_r(T)}{N}\right] = -\frac{E_{v2} + E_{r2}}{kT} \qquad (2)$$

A plot of the left side of (2) against upper level energy for each line, leaving ln(Q/N) as an arbitrary additive constant, should result in a straight line with slope -1/kT. This procedure was carried out for both BN and KL with the results shown in figure 6. Assuming the linear dependence, a weighted least squares fit (weight of zero for S(2) in KL with other weights according to the uncertainty in the observed flux) gave temperatures of 2500(+1500, -700)K for BN and 1400(+1700,-600)K for KL. No correction for reddening was applied.

A qualitative limit to the amount of reddening and saturation is provided by the close proximity of the S(1) and Q(3) lines in figure 6. These lines arise from the same upper level and should plot at the same position regardless of excitation mechanism, so long as saturation effects are negligible. Our neglect of reddening is justified by the overlap of the error bars for S(1) and Q(3). The ratio of ortho to para molecular hydrogen (nuclear spins parallel and anti-parallel

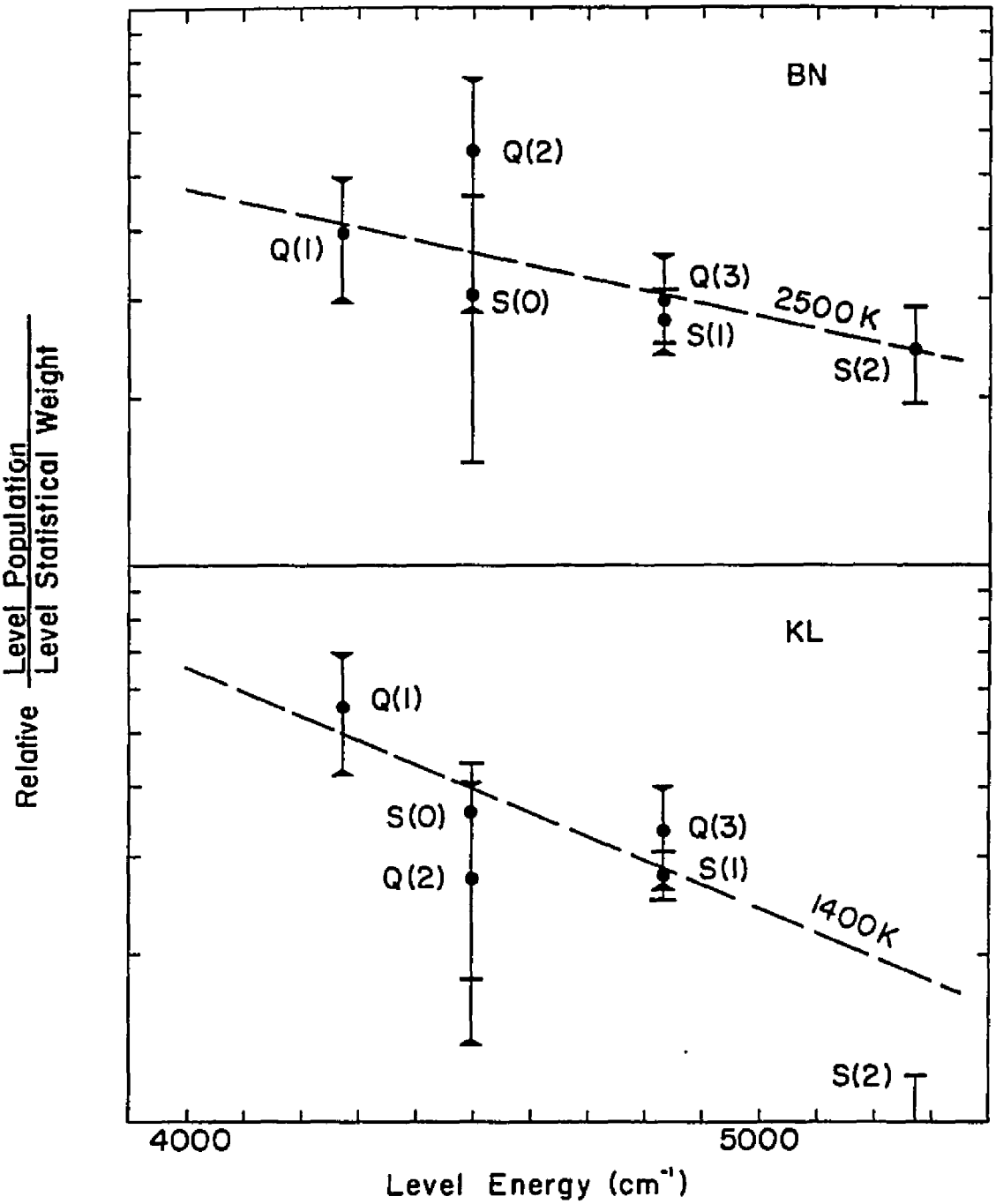

Figure 6. Temperature fit to BN and KL. -- Dotted lines are the weighted least squares fit to the data points. The slope of the lines is -hc/kT. Triangular limit marks refer to error estimates for Q lines, straight marks refer to S lines.

respectively) can also be seen to be near the ratio of 3:1 expected at high temperatures (>700K) since equation (1) assumes population according to strict thermal equilibrium.

Once it was seen that a thermal excitation model was reasonable and a temperature was obtained the ln(Q/N) term in equation (2) could be used to derive a column density of the excited H_2. Using 2000K we derived $N(H_2)$ of 9×10^{18} cm^{-2}. This value was later closely duplicated for the areas around BN and KL by Beckwith, Persson, Neugebauer and Becklin (1978) from a more extensive series of observations of the Orion H_2 emission.

Although not pointed out in our 1976 paper because we had other evidence for thermal population distribution, particle collisions will not guarantee a thermal population unless they are frequent enough to cause the H_2 molecules to undergo several collisional transitions for each spontaneous radiative transition. The small spontaneous transition coefficient of H_2 tends to ease the requirements on temperature and density of the H_2 to produce the needed collisional transition rate but a low inelastic collisional cross section results in a requirement of about $N(H_2) = 10^5$ cm^{-3} at 2000K. It was later noted by some authors that space densities of this order combined with the observed column densities indicate that the excited H_2 is confined to very thin sheets. ($<10^{14}$ cm $\sim$ 7 AU). That is about 10^{-4} of the observed extent of the emission in Orion perpendicular to the line of sight. A clumpy or filamentary geometry may be an alternative to a thin sheet. This point will be discussed in a later chapter. The ease of detection of

these high intensity emission features of H_2 offered the exciting possibility of a new, generally useful probe of the deep interiors of dark clouds. With this opportunity and the encouragement of my thesis advisor I decided to build an instrument suitable for a general survey for large, low surface brightness H_2 emission. After a brief digression into the theory of shock excitation of H_2 I will describe the instrument and the resulting survey.

CHAPTER 3

SHOCK EXCITATION OF H_2

Following the initial detection of H_2 emission several groups began theoretical investigation of possible excitation processes. The principle results of these investigations have appeared in five papers (Hollenbach and Shull, 1977; Kwan, 1977; London, McCray and Chu, 1977; Shull and Hollenbach, 1978; and Shull, 1978). I present here a summary of these results.

Black and Dalgarno (1976), in their study of near ultra-violet fluorescence in H_2, found that after an H_2 molecule had been electronically excited by absorption of a UV photon in its Lyman or Werner absorption bands there was about a 2% probability that the excited molecule would emit an S(1) photon during its cascade back to the ground state. They assumed that molecule-molecule collisions did not significantly alter the level populations among the cascading molecules. Hollenback and Shull (1977) applied the Black and Dalgarno cascade calculation to the observed H_2 emission from Orion and found two difficulties with the mechanism. First, assuming that the dust mixed with the H_2 absorbs 75% of the flux in the 912-1100A region and the H_2 absorbs the remaining 25%, θ^1C Ori, the major near UV source, is too faint by a factor of at least three to explain the observed S(1) intensity. Second, the needed flux level of NUV radiation would probably heat the dust grains in the region of the emitting H_2 to a temperature

(∿100K) at which the formation of new hydrogen molecules would cease. The destruction rate of H_2 from the UV radiation would then be so great that no H_2 would exist in the irradiated region. At NUV flux levels low enough to allow the continued existence of H_2 the S(1) strength would be only 3% of the observed intensity. Kwan (1977) reaches a similar conclusion concerning the energy deficit of θ^1C and also considers the possibility of an NUV source imbedded in the molecular cloud. He finds that the luminosity of the Kleinmann-Low region is consistent with the existence of an NUV source bright enough for the H_2 excitation but then points out that the angular size of the H_2 emission region is incompatible with the lack of a radio detectable HII region at the position of KL. Both Hollenback and Shull and Kwan point out that at higher densities than those assumed for Black and Dalgarno's calculation (10^3 cm^{-3}) the cascade population distribution may be modified sufficiently by collisions, particularly "resonant" inelastic collisions in which, for instance, a molecule with v = 0 collides with a molecule with v = 2 to produce two molecules with v = 1, to enhance the S(1) radiation rate to the observed level. Neither paper completely rules out excitation by NUV radiation; however, both suggest that excitation of the H_2 by collisions in the hot, dense region behind a shock front is the simplest, most direct way of explaining the H_2 emission in Orion. Shull (1978), in a more detailed discussion of the cascade process, also concludes that the explanation of the Orion emission most likely lies elsewhere than with NUV fluorescence.

General Characteristics of Shock Heating

Hollenback and Shull (1977), Shull and Hollenbach (1978) and London et al. (1977) have all carried out detailed calculations of the physical behavior and emitted spectrum of dense molecular clouds where essentially all H is in the form of H_2 in the wake of strong shock fronts. All these groups reach essentially the same conclusions with differences occurring mainly in the limiting velocities of the shocks due to poorly known collisional dissociation rates for H_2. The general characteristics of the shock heating process are as follows.

1. There is minimum pre-shock density, $n_0 \geq n_{crit} \sim 10^5$ cm^{-3}, below which radiative processes dominate inelastic collisions in the population of the H_2 energy levels and prevent the establishment of a Boltzmann distribution, at least among the levels producing the observed radiation.
2. Shock velocities above $V_s = 8$ km s^{-1} are needed to produce the observed intensities in Orion but velocities above about 21 km s^{-1} will dissociate so much H_2 that no H_2 radiation will appear.
3. In the immediate post shock region the vibrational and rotational modes of the H_2 molecules have not been excited, the translational temperature is $\sim 5300\text{K}(V_s/10 \text{ km s}^{-1})^2$, and $n = 4n_0$. The difference in the internal temperature and the translational temperature is due to the large difference between the elastic and inelastic collisional cross sections of H_2. Further behind the shock the internal modes of the H_2 are

excited and the temperature drops to ∿65% of the immediate post shock temperature while n goes up to $7n_0$. This temperature structure is slightly modified for immediate post shock temperatures above 5000K where collisional dissociation of the H_2 becomes important. In this case, at least up to shock velocities ∿21 km s^{-1}, dissociation rapidly cools the gas to a translational temperature of ∿5000K. After the internal modes of the H_2 are thermalized there is a relatively large radiative cooling region (∿3 × 10^{12} cm for $n_0 = 10^5$ cm^{-3} and V_s = 10 km s^{-1} according to London et al., 1977).

4. The relative intensities of the vibration-rotation lines around 2 μ are not strongly influenced by the shock velocity. The temperature indicated by the line ratios is always between 1600K and 2000K.
5. The pre-shock density needed to produce the S(1) intensity observed in Orion ranges from $n_0 \sim 5 \times 10^5$ cm^{-3} at $V_s \sim 8$ km s^{-1} to $n_0 \sim 10^5$ at $V_s \sim 21$ km s^{-1}.
6. Cooling by CO and other molecules is insignificant until the temperature of the post shock region drops below about 500K because CO is so much less abundant than H_2. No significant radiation is expected to be seen from the CO, at least from low J transitions, due to the strong absorption of the great majority of cold CO.
7. Magnetic fields of intensities expected in molecular clouds do not have a great effect on the above results.

All authors found some difficulty in producing a shock of the required intensity over the whole region of the H_2 emission in Orion. Kwan found the electron density in the HII region to be several orders of magnitude too small to maintain a pressure behind the shock sufficient to prevent its rapid decay and London et al. found that although a stellar wind from θ^1C Ori could possibly sustain the shock, this resulted in an uncomfortably high mass loss rate from θ^1C. Radiation pressure from θ^1C is also insufficient to maintain the shock. The energy source in KL is not luminous enough to produce a mass loss rate large enough to drive the required shock. Kwan suggests that an explosive event such as proposed by Kwan and Scoville (1976) could possibly supply the shock. If the H_2 emission originates from within the molecular cloud instead of directly on the surface nearest the earth extinction due to dust will tax all possible sources of energy even more severely.

CHAPTER 4

SURVEY INSTRUMENT DESIGN AND OPERATION

When the decision was made to pursue a general survey program for 2 μ H_2 emission the question of suitable instrumentation arose immediately. Based on what was known about celestial H_2 sources a survey instrument needed state of the art signal to noise qualities in its detector, the lowest possible internal losses and a large through-put both to be effective on large, low surface brightness sources like the Orion source and to increase the search rate. A through-put of $A\omega \sim 3 \times 10^{-4}$ cm^2 sr (10 mm beam at f/45 which gives ∼30" field of view on the 154 cm telescope at the Catalina site of The University of Arizona) was considered reasonable. This beam size would receive the bulk of the energy from extended sources of size comparable to the Orion source, giving the instrument a large advantage in sensitivity over smaller beam sizes, while the large beam would be no disadvantage so long as detector noise and background noise could be kept under control. Previous experience with indium antimonide detectors and a calculation of the expected background level indicated that the noise problem could be managed.

Selection of Technique

I first considered using existing instrumentation. The LPL FTS instrument used for the initial detection of the H_2 in Orion had the

advantages of wide spectral coverage, high resolution and the unbeatable Felgett advantage when observing many spectral points. Unfortunately it had somewhat high internal losses (∿70%) and its wide spectral coverage and accompanying Felgett advantage could not be used with a wide beam detector due to the high level of background radiation admitted through a wide spectral pass band. Additionally the FTS system used a time consuming and expensive data reduction process, required a large amount of man power in its operation and was heavily dedicated to other programs. The FTS was well suited to studying known H_2 sources but not to finding new ones. No other existing instruments were found which met the survey instrument requirements.

Three techniques were considered to implement the desired performance in a new survey machine: 1) a grating spectrometer, 2) a prism spectrometer, and 3) an interference filter spectrometer. A grating spectrometer could have been made to work with the required resolution and through-put but would have been physically large (∿1 meter). This is a fairly large instrument for cassegrain use in absolute terms and since I was considering cooling the whole instrument to help eliminate background noise the grating spectrometer was unattractive. A prism spectrometer using quartz or calcium fluoride as the dispersing element needed a dimension on the order of 10 meters to provide the needed resolution and through-put and was also rejected. Interference filter spectrometers using circular variable filters of the variety commonly available could not provide adequate spectral purity at the desired through-put. CVF's typically require a radial

slit mask to insure high resolution and spectral purity. Such a slit could not accommodate the 10 mm input beam without a complicated and lossy image slicing arrangement. The technique that best met the needs of the survey instrument was a tilting filter spectrometer. In this instrument a narrow band interference filter is mounted so that its effective pass band can be shifted by tilting the plane of the filter with respect to the light beam from the telescope. This dissertation project is not an original application of this type of spectrometer. Eather and Reasoner (1969) built a tilting filter spectrometer for airglow observations in the visible region of the spectrum. The H_2 survey machine is, to the author's knowledge, the first application of a tilting filter spectrometer to astronomy.

Filter Performance

The necessary and desirable characteristics of an interference filter for the H_2 survey machine were:

1) A diameter of 38 mm to accommodate an unvignetted 15 mm field of view in an f/45 beam when the filter and its mounting structure are tilted 45°.
2) Passband at normal incidence centered at 2.145 microns.
3) Band pass $\leq$0.001 μ full width at half maximum at normal incidence and $\leq$0.012 μ fwhm at 40° incidence. This is adequate to discriminate against nearby lines, notably the 2.113 μ line of HeI near H_2 1-0 S(1) at 2.122 μ.
4) Variation of center wavelength over the filter area <0.002 μ.

5) Transmission $\geq$50% at center of pass band (design goal $\geq$70%). This peak transmission makes the tilting filter monochromator a viable alternative to other techniques.

6) Variation of center wavelength with angle of incidence at least 3% toward shorter wavelengths from normal incidence to 40° (design goal 6%).

7) Shift of center wavelength with temperature $\leq$0.006 μ between 0C and -56C.

A filter meeting these specifications was not easy to obtain. Interference filters with 1/2% bandpass and 70% central transmission are tricky to produce and most filter manufacturers go out of their way to avoid the performance specified in requirement 6. (The variation of central wavelength with angle of incidence is normally held to a minimum with the use of high refractive index materials in the multi-layer coatings.) Of the several manufacturers invited to bid for this filter only one, Spectrum Systems in Waltham, Massachusetts, was willing to meet the specifications at a reasonable price.

The characteristics of the filter actually obtained from Spectrum Systems are detailed in figures 7 through 11. The center wavelength at normal incidence and 0C was 2.1413 μ. The filter's passband is somewhat wider than the specified requirements but this seemed the best that could be done with a central transmission greater than 50%. I actually received two sets of four filters from Spectrum Systems. The first set had 30% better resolution but only 37% transmission and a smaller wavelength shift with tilt angle than the second set.

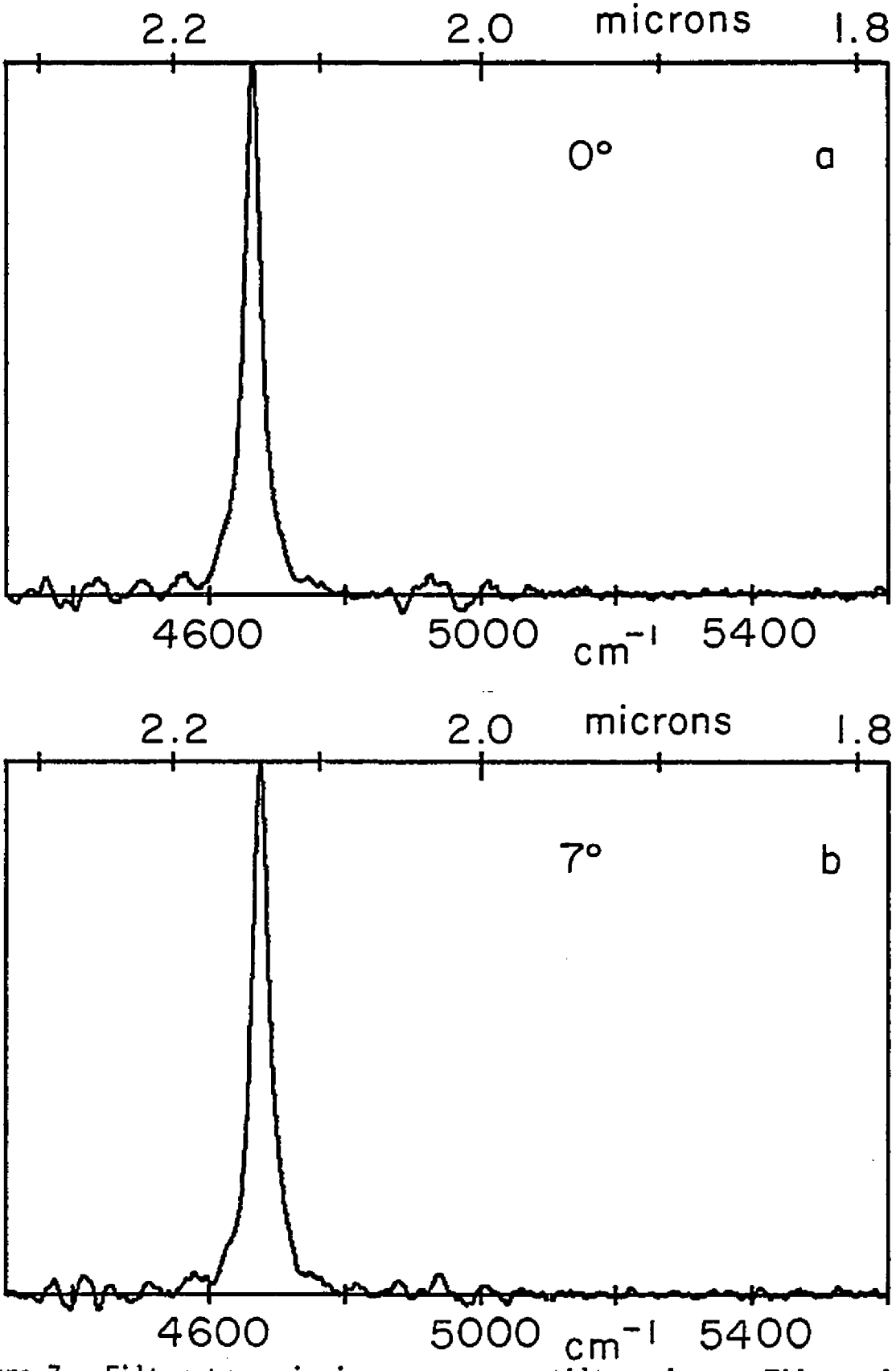

Figure 7. Filter transmission curves vs. tilt angle. -- Tilt angle is shown in each subfigure. The vertical axis is arbitrarily normalized but is the same for all subfigures.

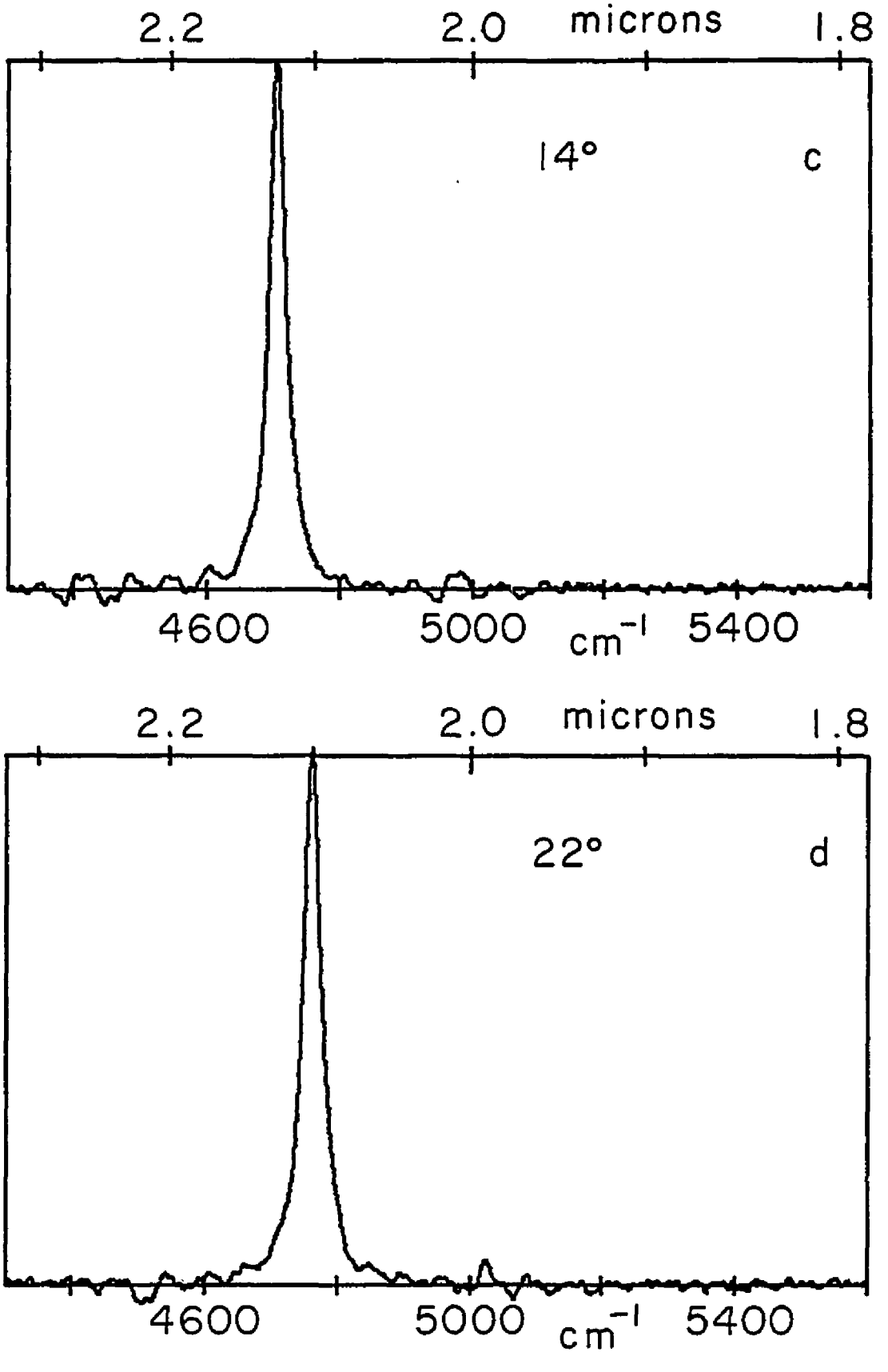

Figure 7. Filter transmission curves vs. tilt angle (Continued)

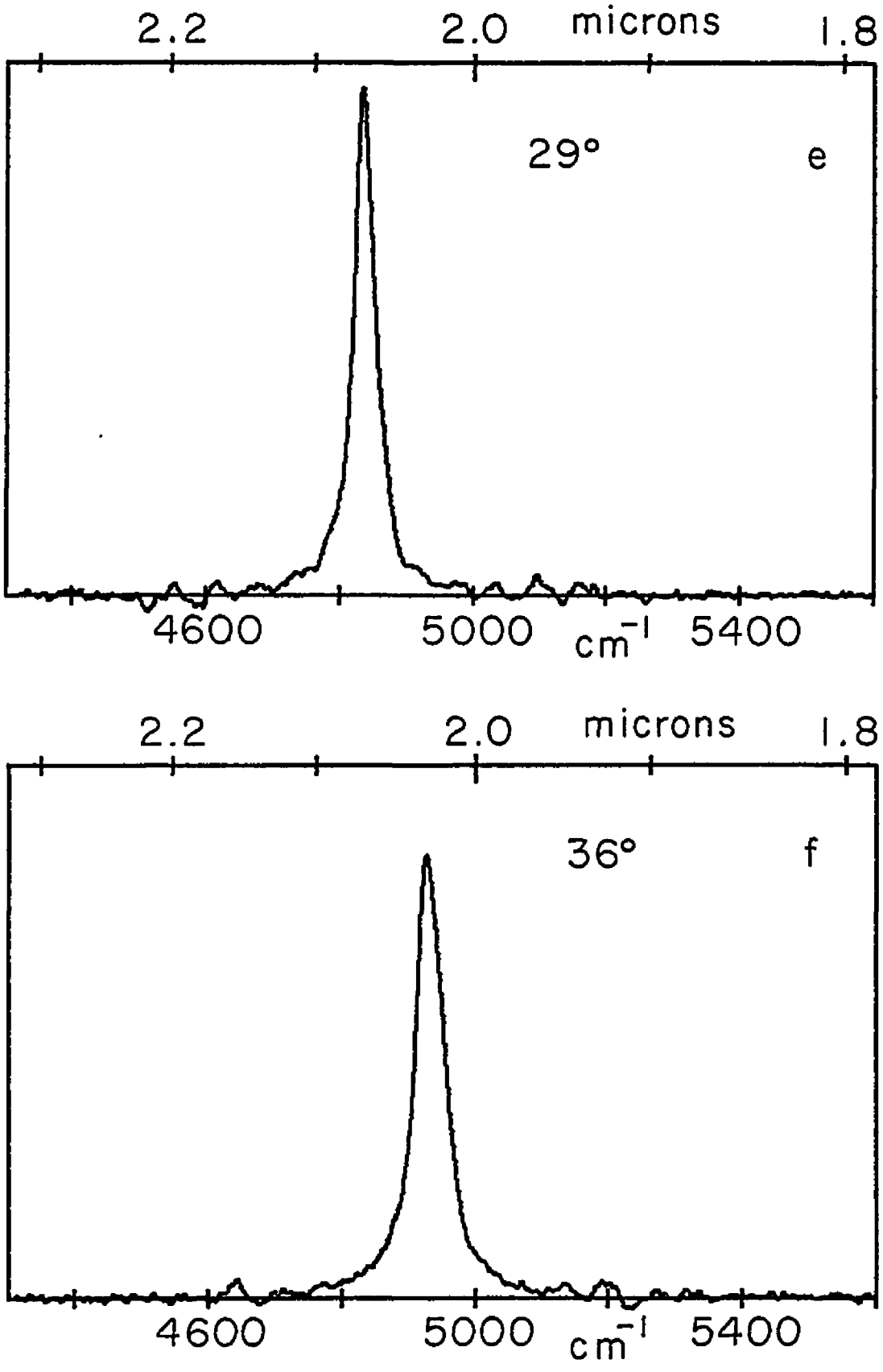

Figure 7. Filter transmission curves vs. tilt angle (Continued)

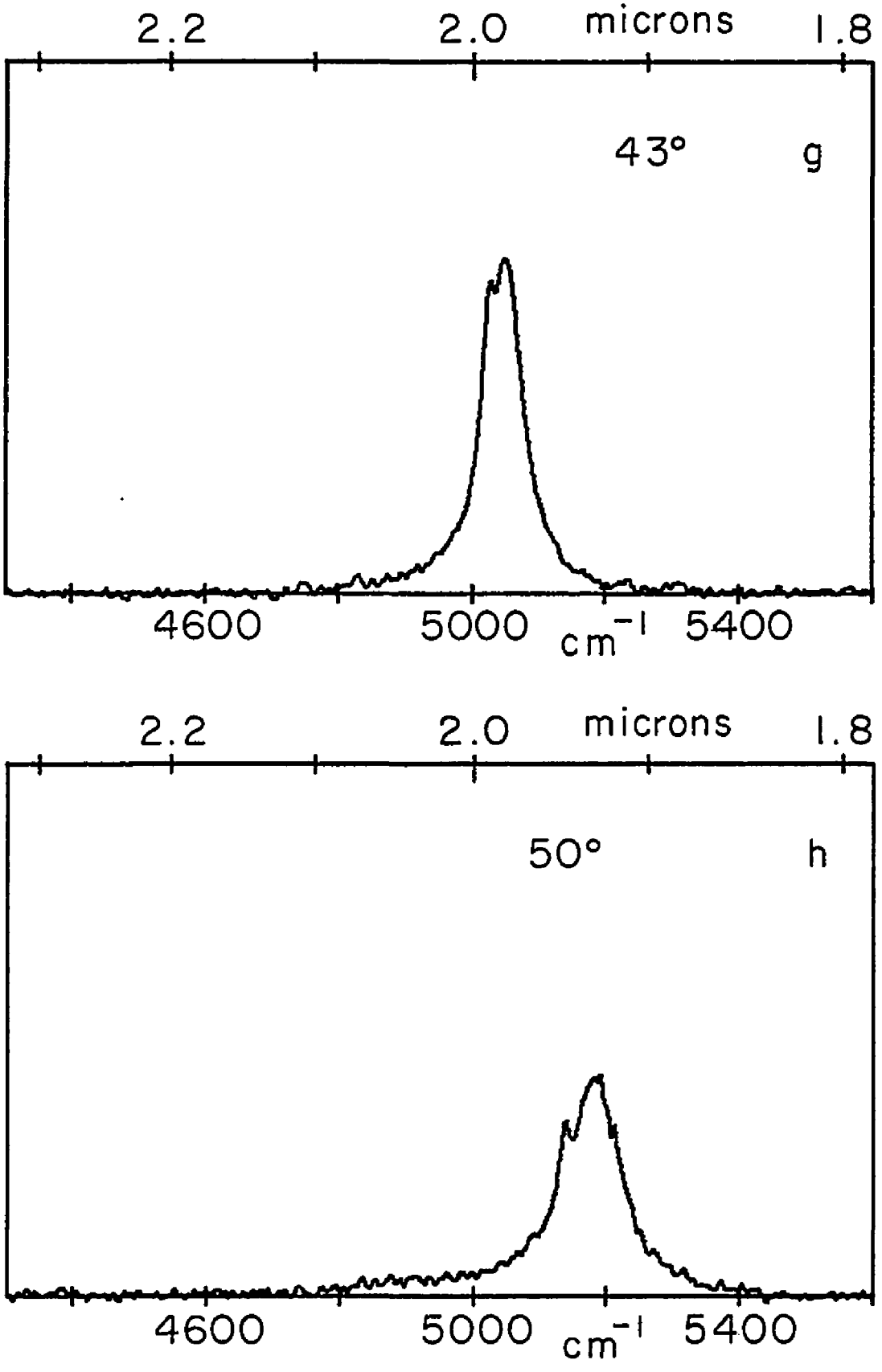

Figure 7. Filter transmission curves vs. tilt angle (Continued)

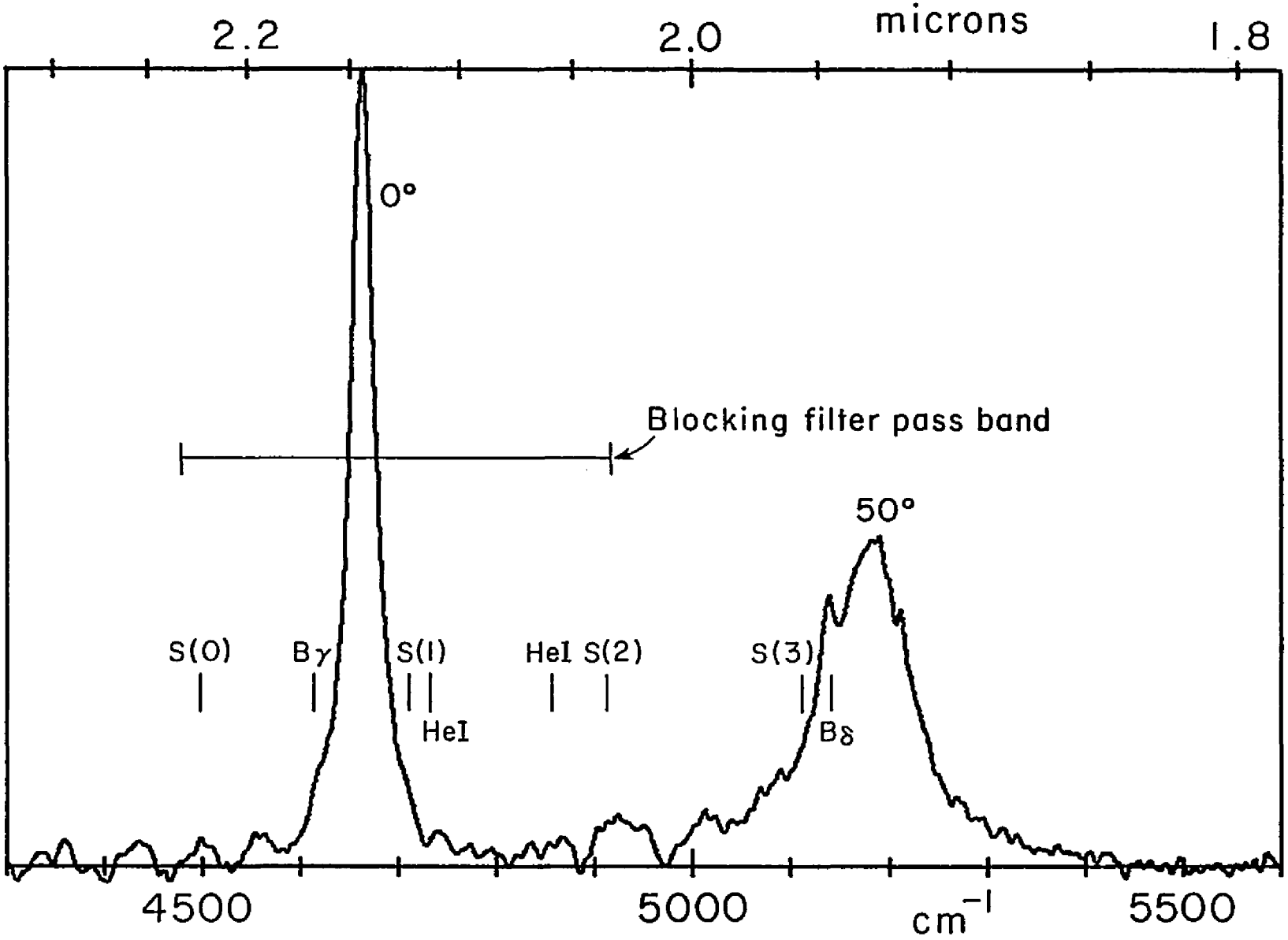

Figure 8. Composite monochromator range diagram. -- The filter transmission curves for normal incidence were added to produce a curve showing the effective range of the monochromator. The positions of several important spectral lines are indicated and the blocking filter pass band is shown.

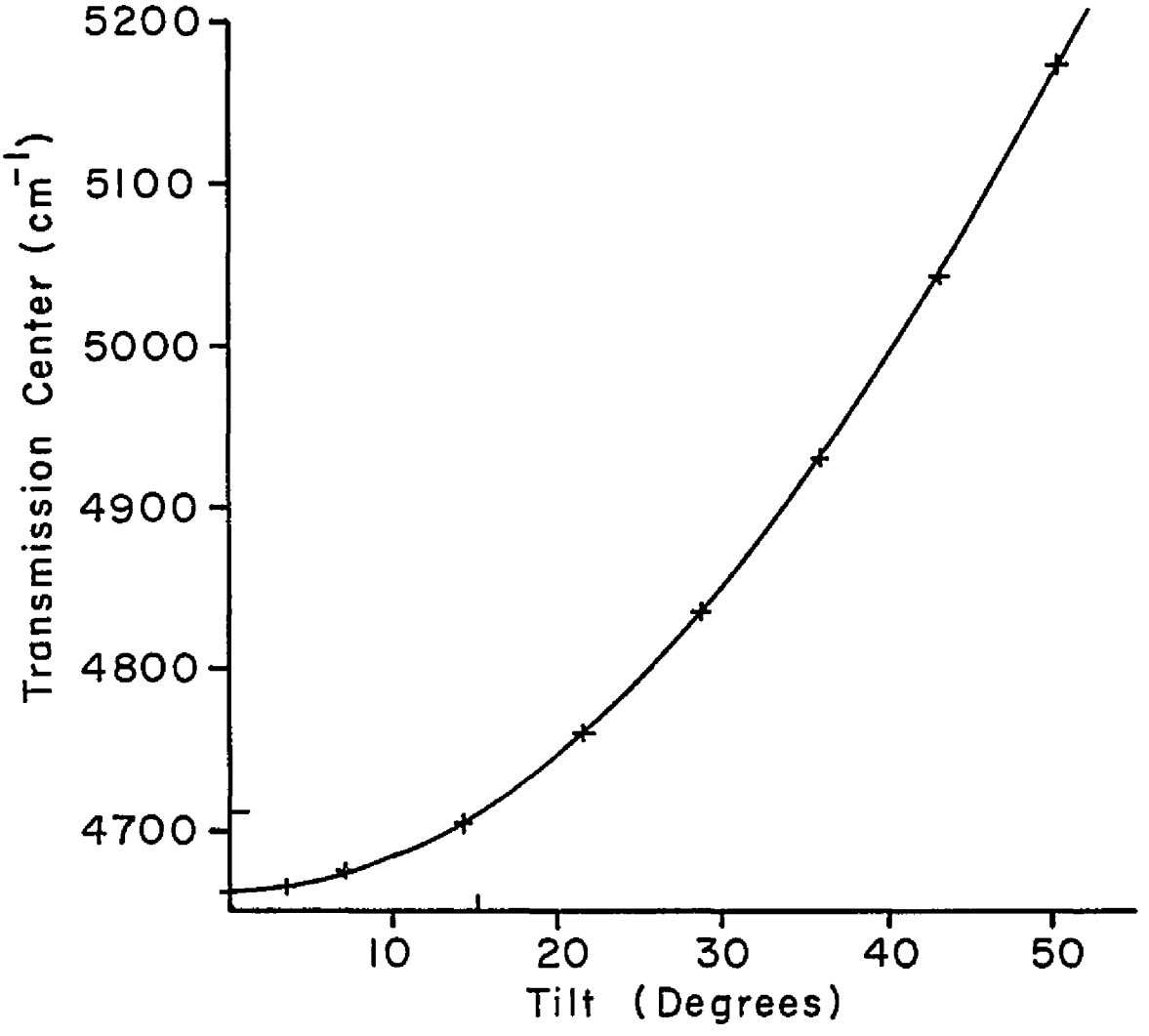

Figure 9. Transmission center vs. tilt angle calibration curve. -- The wave number of the 1-0 S(1) line (4712 cm^{-1}) and the corresponding tilt angle are indicated by tic marks.

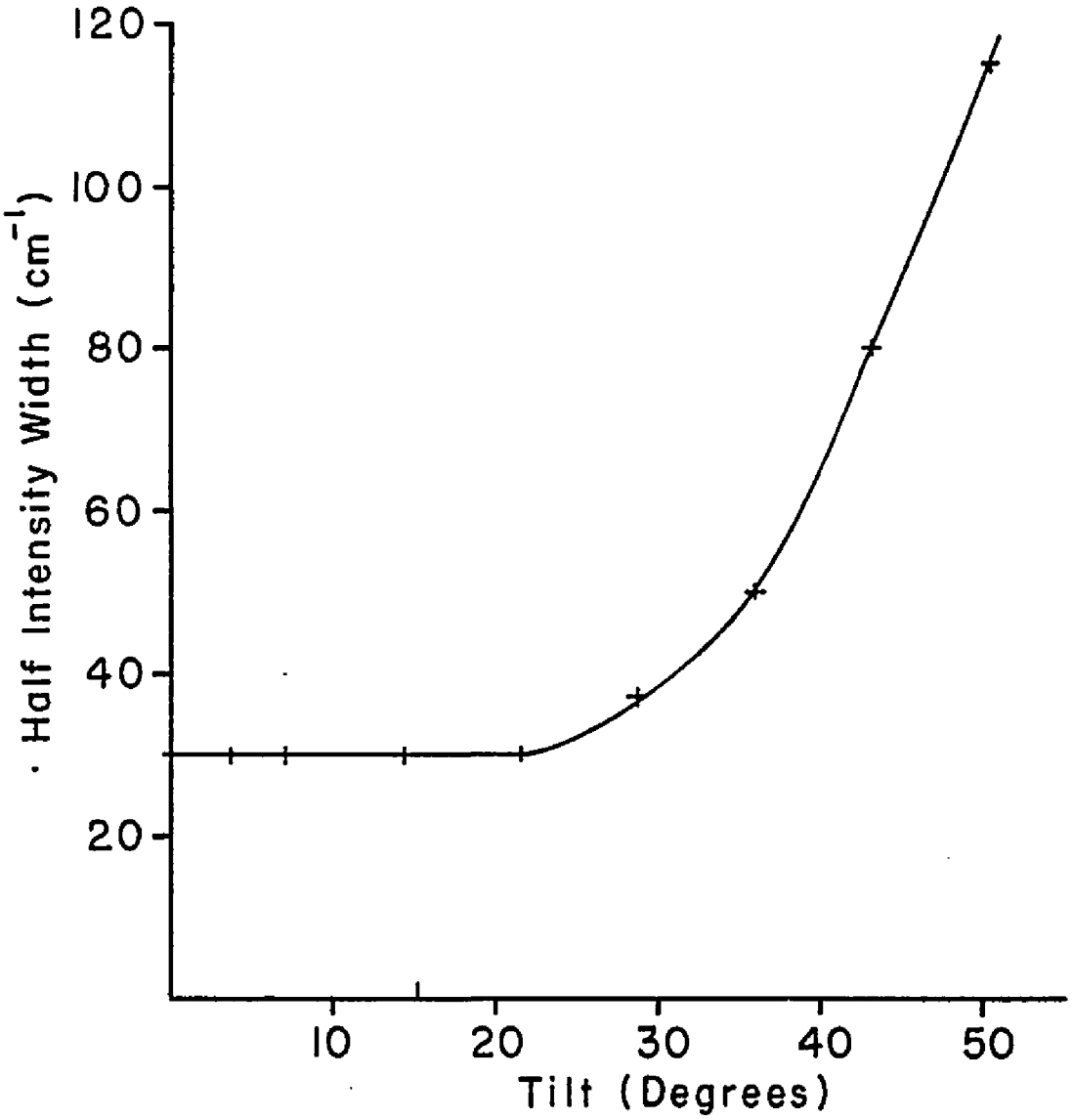

Figure 10. Half intensity width vs. tilt angle. -- The tilt angle for the 1-0 S(1) line is indicated by a tic mark.

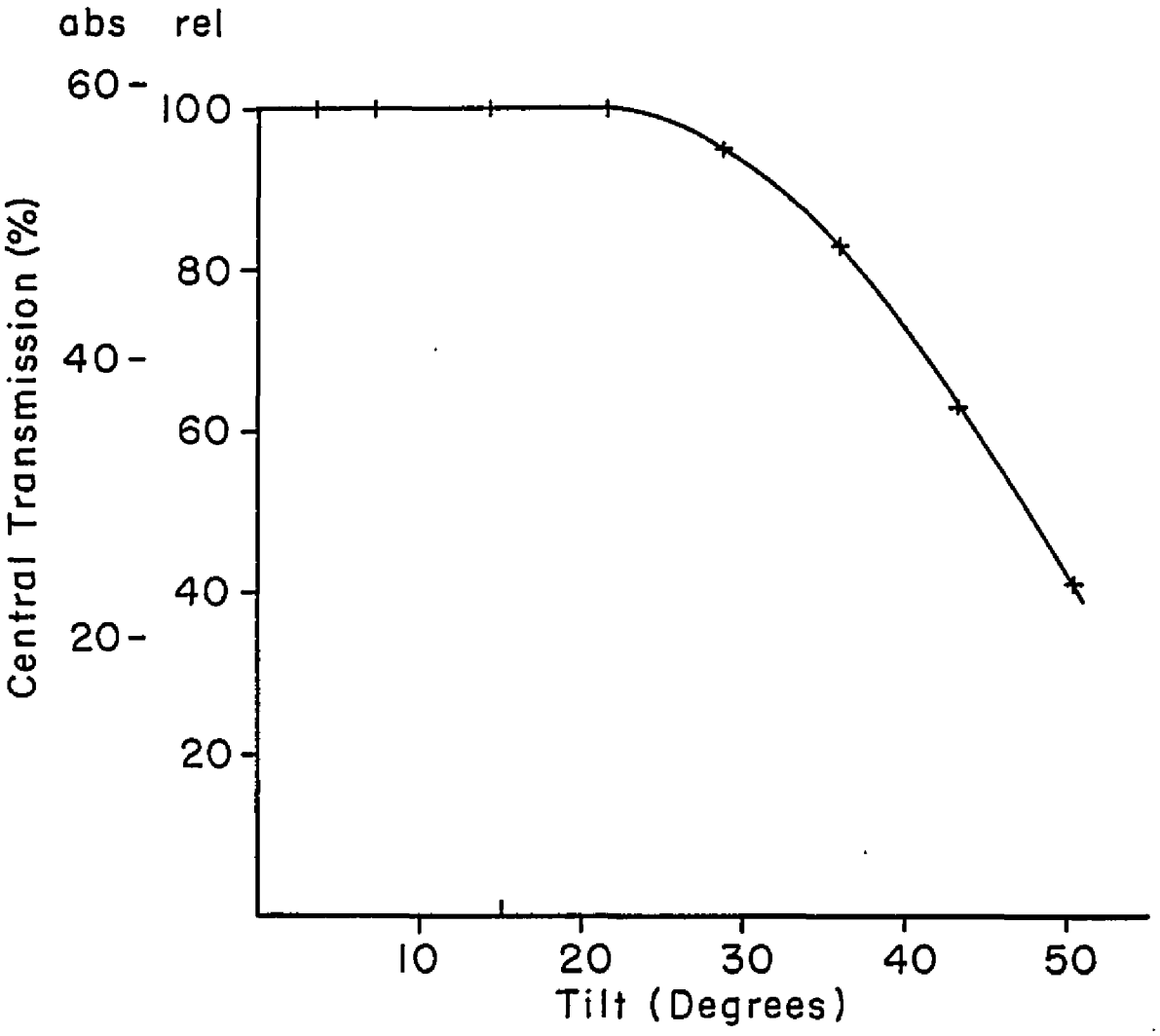

Figure 11. Central transmission vs. tilt angle. -- The tilt angle for the 1-0 S(1) line is indicated by a tic mark.

I elected to use the broader filter in favor of the higher transmission. The variation of central wavelength with angle of incidence met the design goal and the shift of the passband with temperature was only -0.0009 μ from 23C to 0C which extrapolates to -0.002 μ from 0C to -56C. Note that the S(1) line at 2.122 μ falls on the flat part of the width versus angle of incidence curve (figure 10). I am indebted to Drs. Harold Larson and Uwe Fink of the Lunar and Planetary Laboratory, University of Arizona, for the use of their fourier transform spectrometer to obtain the calibration curves. The optical system used to produce the calibration spectra closely approximated the f/45 input beam which was used at the telescope so no calibration or band pass errors were introduced by the divergence of the telescope's output beam.

Instrument Configuration

Figure 12 is a schematic diagram of the entire optical system of the survey instrument. The box housing the filter was designed to sandwich in between the detector dewar and our standard photometer guide boxes so that the filter could be used with systems other than the survey instrument. Included in the filter box was a toothed chopper wheel. Dr. Wade Poteet supplied the design of the excellent, yet simple, servo speed control used to drive this chopper wheel. A 1000 steps per revolution stepper motor was mounted to the outside of the filter box so that its drive shaft protruded into the interior of the box. The filter mounting structure was fastened to the end of the stepper drive shaft so that the center of the filter was positioned in the center of the light

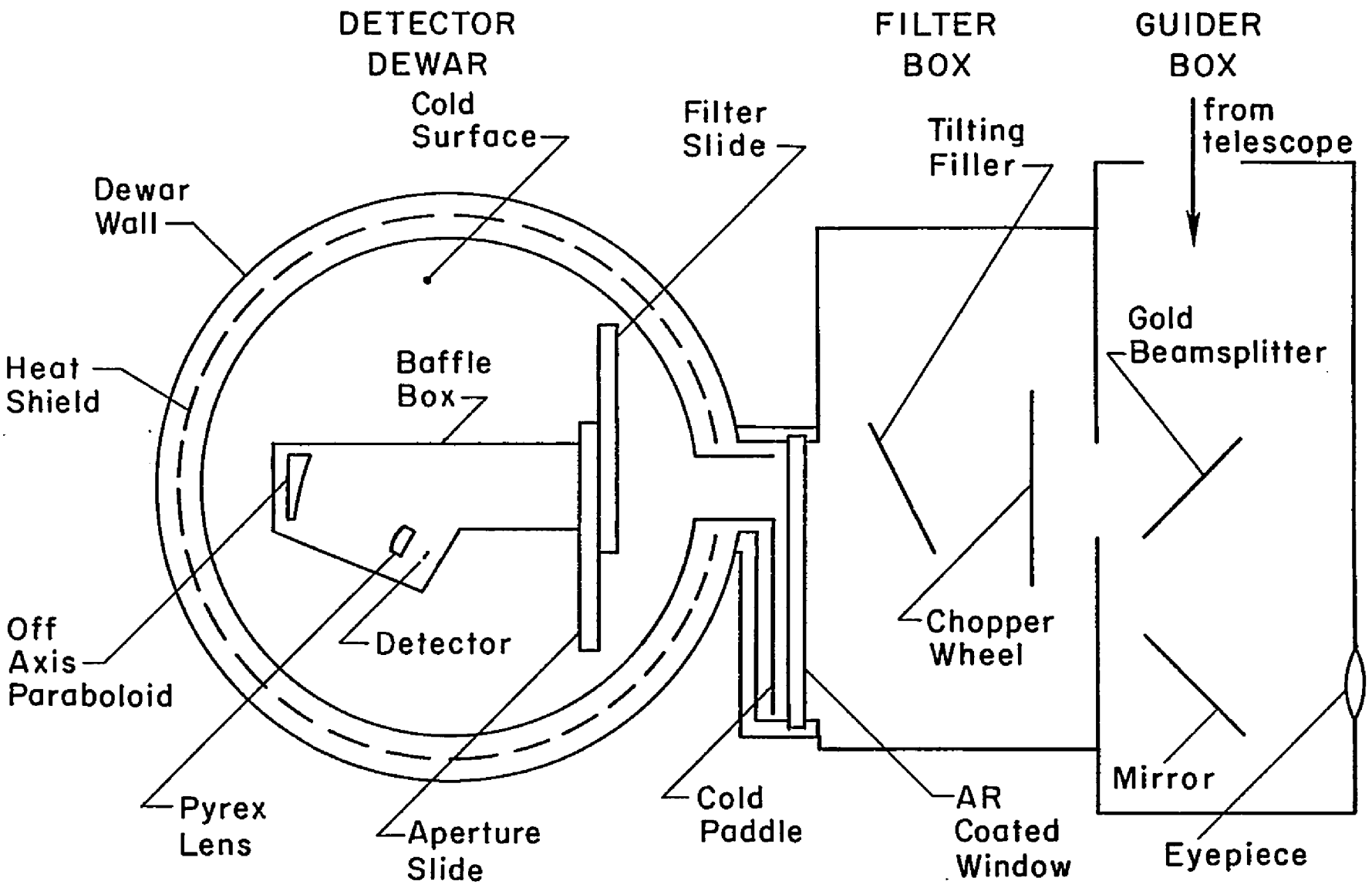

Figure 12. Schematic diagram of detector, filter and guider assembly.

beam from the telescope. The filter itself was held in a secondary mounting plate which was hinged on an axis parallel to the stepper drive axis within the structure fixed to the stepper drive shaft. A solenoid driver was arranged to move this secondary plate allowing the filter position to be rapidly modulated from the position selected by the stepper motor thus producing a frequency chopping monochromator. A precision potentiometer was attached to the stepper motor shaft to allow the absolute position of the filter to be monitored. A logic system which allowed flexible automatic control of the stepper motor was designed and constructed by R. Sparrold as a senior project in Electrical Engineering.

Detector Selection

The other major part of the H_2 survey instrument is the detector system. A liquid nitrogen cooled indium antimonide photo-diode operating in the photovoltaic mode was then the state of the art 2 μ infra-red detector and was chosen for use in this system. An InSb photo-diode converts infra-red radiation into electrical signals by absorbing a photon in the depletion zone at the P/N junction of the diode which creates an electron-hole pair. The contact potential of the P/N junction draws the electron to one side of the junction and the hole to the other, causing a potential difference to appear across the photo-diode. In practice the InSb photo-diode is used as a current generator rather than a voltage generator. This permits both sides of the diode to be maintained at the same potential, preventing the sizable series resistance of the diode from generating any Johnson voltage

noise. The equivalent circuit of the photo-diode as a current generator and a series resistance is shown in figure 13. Also in figure 13, the photo-diode is shown feeding the input of a transconductance amplifier, that is, an amplifier whose output voltage is proportional to its input current, which satisfies the requirement that both sides of the diode be at the same potential. The operational amplifier in figure 13 tries to maintain equal potential at its + and - inputs. When the photo-diode's current generator delivers current to the - input of the op amp the potential of the - input changes with respect to the + input. The op amp then changes its output voltage, V_o, to produce a current through R_f which exactly cancels the photo-diode's current and returns the - input to the same potential as the + input. This transconductance amplifier produces an output voltage proportional to the input current, I_λ, according to the formula

$$V_o = I_\lambda R_f \quad . \tag{3}$$

The Johnson current noise in the diode's equivalent resistance, R_d, is given by

$$I_{nd} = \sqrt{4kT/R_d} \tag{4}$$

and the amplifier output noise due to this current noise is

$$V_{nd} = R_f\sqrt{4kT/R_d} \tag{5}$$

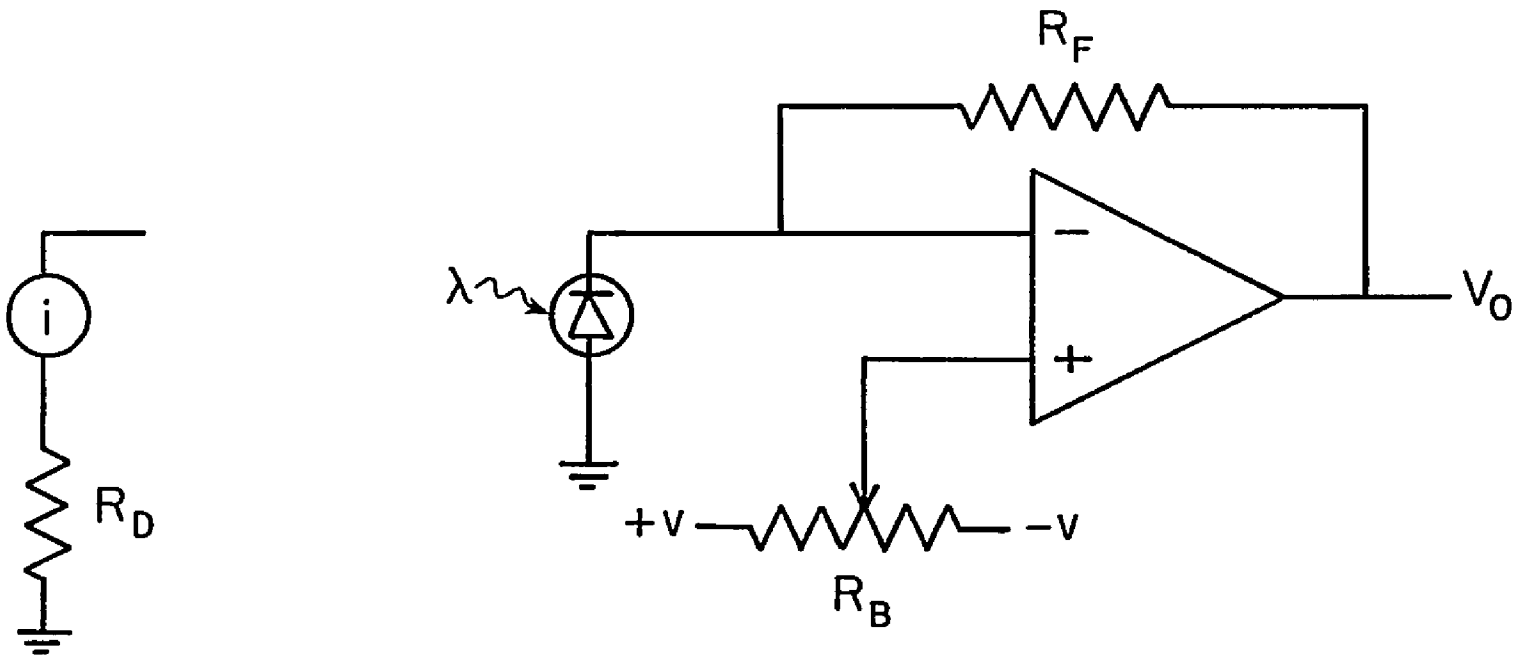

Figure 13. Basic InSb pre-amplifier. -- A more complete design similar to the one used in the survey detector system is described in Hall, Aitkins, Joyce and McCurnin (1975). R_B is used to adjust the detector bias voltage for lowest noise.

where T is the absolute temperature of the diode. The feedback resistor itself contributes a Johnson voltage noise to the amplifier output given by

$$V_{nf} = \sqrt{4kTR_f} \tag{6}$$

where T is the temperature of the feedback resistor, so the total Johnson noise present at the output of the amplifier is given by

$$V_n = \sqrt{4kT(R_f + R_f^2/R_d)} \tag{7}$$

if the temperatures of the diode and feedback resistor are the same. With this noise the signal to noise ratio for a fixed photon flux is

$$S/N = \frac{I_\lambda \sqrt{R_f}}{\sqrt{4kT(1 + R_f/R_d)}} \quad . \tag{8}$$

The derivative of this function with respect to R_f is positive for positive values of R_f so large values of R_f are desirable to increase the signal to noise ratio. If $R_f >> R_d$, equation (8) becomes

$$S/N = \frac{I_\lambda \sqrt{R_d}}{\sqrt{4kT}} \quad . \tag{9}$$

Equation (9) shows that the noise due to the feedback resistor can be neglected if $R_f >> R_d$ and indicates that every effort should be made to increase R_d. Four ways to increase the detector resistance, R_d, are known: 1) make the intrinsic detector resistance high in the manufacturing process, 2) cool the detector (which has the additional advantage of reducing T in equation [9]), 3) subject a cooled detector to an intense flux of photons of wavelength $\sim$1 μ for several minutes before using it to detect faint sources (J flashing) and 4) make sure that the detector becomes and stays very clean during its operation.

My detector selection procedure began with detectors which were chosen by their manufacturer for high intrinsic impedance. I then evaluated their response to treatments 2 through 4. Treatment 3, cooling the detector, was accomplished by not only mounting the detector in a vacuum dewar cooled by liquid nitrogen but additionally by reducing the pressure within the cryogen vessel to bring the liquid nitrogen to its triple point at 65K. With a 1 cm input aperture, an f/45 input beam, a background temperature of 273K, a detector temperature of 65K and a spectral passband of 2.244 μ to 2.043 μ, as used in the survey instrument, the maximum useful R_d is 3.1×10^{10} ohms. Above this value the background radiation from the telescope and atmosphere produces more noise than the detector itself. To further reduce the noise in the final electrical output of the detector system the input radiation is modulated at a convenient frequency and the preamplifier output is put through a very narrow bandwidth filter, usually a synchronous rectifier. (This is true even in a fourier transform spectrometer,

though the synchronous rectification then takes place in the fourier transform mathematics.) For this reason my selection was also made for best noise qualities at 10 Hz. This frequency being near the preamplifier roll off frequency.

Two 0.5 mm round detectors with unflashed 77K impedances $>10^9$ ohms were obtained from Santa Barbara Research Corporation. The better of these detectors displayed a maximum impedance of 2×10^{10} ohms when J flashed and cooled to 65K. The measured noise density produced by the detector system in its operating configuration was 75 uv $Hz^{-\frac{1}{2}}$ at 10 hz with $R_f = 6 \times 10^{10}$ ohms; equivalent to an NEP of 1.2×10^{-15}w $Hz^{-\frac{1}{2}}$ at 2.122 μ. This noise is somewhat greater than the calculated value for pure Johnson noise of 30 uv $Hz^{-\frac{1}{2}}$, but it is difficult to achieve Johnson noise limited operation with detector impedances over 10^{10} ohms. This detector was judged acceptable for the survey instrument.

Detector Optical System

The detector optical system is pictured in figure 12. A Fabry optical system was chosen for the usual reasons of the elimination of noise due to image motion on the detector and to allow the field of view of the detector system to be changed easily. The image plane of the telescope falls on the aperture slide near the window of the dewar. The off axis paraboloid and the small lens focus an image of the telescope's primary mirror on the detector. The focal length of these optics is carefully matched to the detector size so the image of the primary just underfills the detector. (The secondary of a properly designed infra-red telescope is slightly too small so that the edges are

cut off the virtual image of the primary formed by the secondary. In this way the hot parts of the telescope structure around the primary are not imaged on the detector.) The aperture slide contained apertures of diameter 7 mm, 10 mm, and 12 mm. The diameter of the off axis paraboloid was 15 mm to safely accept an f/45 beam from the 12 mm aperture. These apertures gave an actual maximum through-put of $A\omega = 4.4 \times 10^{-4}$ cm^2 sr.

A considerable amount of effort was put into the design of the Fabry optical system. In order to achieve the desired through-put it was necessary to focus the energy on the detector at a final f ratio of f/1.5. The size of the detector mounting substrate precluded the use of on axis optics so several alternative off axis systems were evaluated. I developed a relatively simple computer program to ray trace these alternative optical configurations. The simplest alternative used the configuration in figure 14a with a sphere as the off-axis element. Neither this configuration nor the arrangement in 14b with a sphere produced images of adequate quality. (See figure 15.) An off axis paraboloid for use in figure 14a was prohibitively expensive to produce so the optical system actually used was that of figure 14b with an off axis paraboloid. The lens was made of Corning 7740 pyrex which had adequate transmission at 2.1 μ in the thickness used (∿90%). The final performance of the detector optics was quite good. The beam pattern had a flat top of the expected size and quite steep sides.

A cooled blocking filter was incorporated in the filter slide (figure 12) to eliminate unnecessary background radiation on the

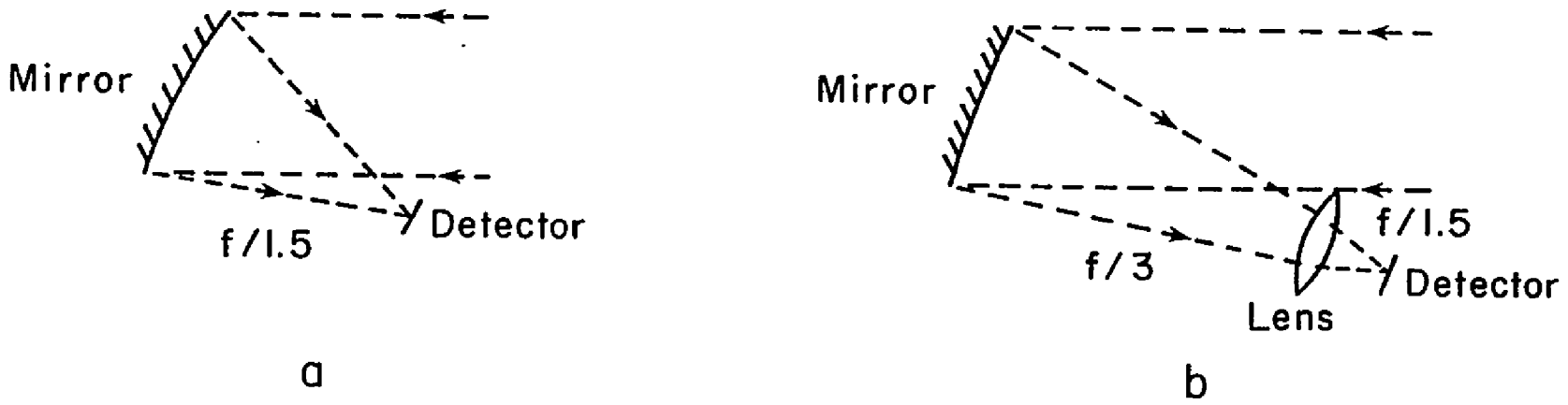

Figure 14. Alternative off-axis optical systems. -- The system in a puts much more stringent requirements on the off-axis element than the system in b which uses an additional lens to demagnify the image. The detector is shown tilted out of the image plane which, in a at least, is normal to the input beam. For a large detector this would be significant but ray tracing showed no great effect for a 0.5 mm disc.

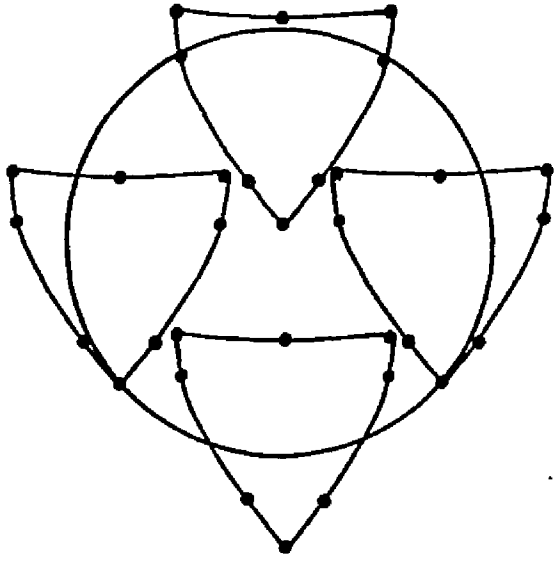

a

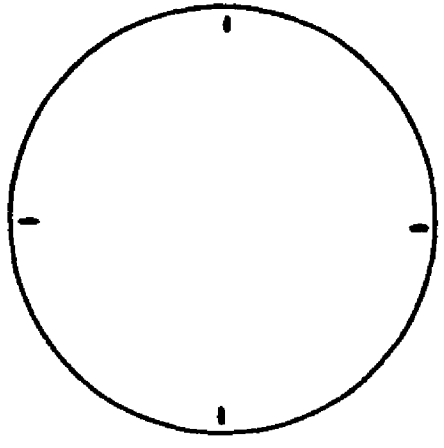

b

Figure 15. Ray tracing results. -- Part a shows the ray tracing results using a spherical off-axis element in the configuration of figure 14, part b shows the results with the actual off-axis paraboloid and lens used in the detector system. The images of four cardinal points at the edge of the telescope primary were computed in each case. Each triangular figure in a is the locus of rays from one of the points on the edge of the primary which were reflected from the edge of the off-axis sphere. The filled dots are a set of individual rays which were evenly spaced around the edge of the off-axis sphere. Rays reflected from the central parts of the sphere fell generally within the triangular figure. Similarly the small ellipses in b are the images of the cardinal points on the primary when an off-axis paraboloid is used. The circles represent the detector's active area.

detector. Assuming a 1% shift to shorter wavelengths upon cooling to 77 K the blocking filter had a central transmission of 82% in a passband of 2.043 μ to 2.244 μ fwhm. The passband maintained 95% of the central transmission from 2.051 μ to 2.228 μ. With 300K background and $A\omega = 3.05 \times 10^{-4}$ cm^2 sr this passband gives a background NEP of 1.0×10^{-15} w $Hz^{-\frac{1}{2}}$. At 273K the NEP would be 3.5×10^{-16} w $HZ^{-\frac{1}{2}}$. My detector system was slightly detector noise limited for a 300K background with its NEP of 1.2×10^{-15} w $Hz^{-\frac{1}{2}}$.

Operating Modes and Procedures

When operating in the frequency chopping mode the tilting filter is flipping back and forth at 10 Hz through an angle of about 4.3 degrees. Reflections of external and internal radiation sources off the filter surface and into the detector represent a potentially serious source of noise. Careful attention to making the photometer system light tight eliminated the problem for external sources. Internal radiation sources, however, proved to be more of a problem. The cold paddle in figure 12 was not included in the original detector configuration and the detector could see the interior wall of the filter box by reflection in the filter. Small temperature variations along the wall would produce a large and unpredictably variable offset in the detector output in the frequency chopping mode. The source of this offset was verified by noting that heating the outside of the offending wall of the filter box with my hand or cooling it with the boil off from some liquid nitrogen would drastically affect the offset. This problem was reduced by an order of magnitude to a quite manageable level by the addition of the

cold paddle and window, anti-reflection coated for 2.1 μ. The paddle was made of aluminum, coated with 3M "Nextel" flat black paint and attached to the cold surface of the dewar. Its geometry was so arranged that the detector saw only the paddle reflected in the filter for all filter angles used in the survey. The interference filter had a quite high reflectivity for radiation outside its passband (>90%) so the combination of the cold paddle and the AR coated window not only nearly eliminated the offset drift problem but also provided a background reduction equivalent to cooling the entire filter box. Unfortunately the detector itself didn't have low enough noise to take full advantage of this background reduction. A calculation of the radiative heat input to the paddle indicated that the extra heat load on the dewar cold surface would be only a fraction of a watt, easily handled by a nitrogen cooled dewar, and that the temperature at the warm end of the paddle would be well below 100K.

A block diagram of the entire photometer system will be found in figure 16. Three modes of operation of the photometer were available. As noted before, the filter angle could be modulated over a small interval to produce frequency chopping in the output beam of the filter. In addition two methods of spatial chopping could be employed. The energy from the telescope could be compared to an ambient temperature source in the form of the toothed chopper wheel within the filter box or the sky plus source energy could be compared to the sky alone using the chopping secondary of the telescope. In all modes the electronics driving the modulating element produced a synchronization signal for

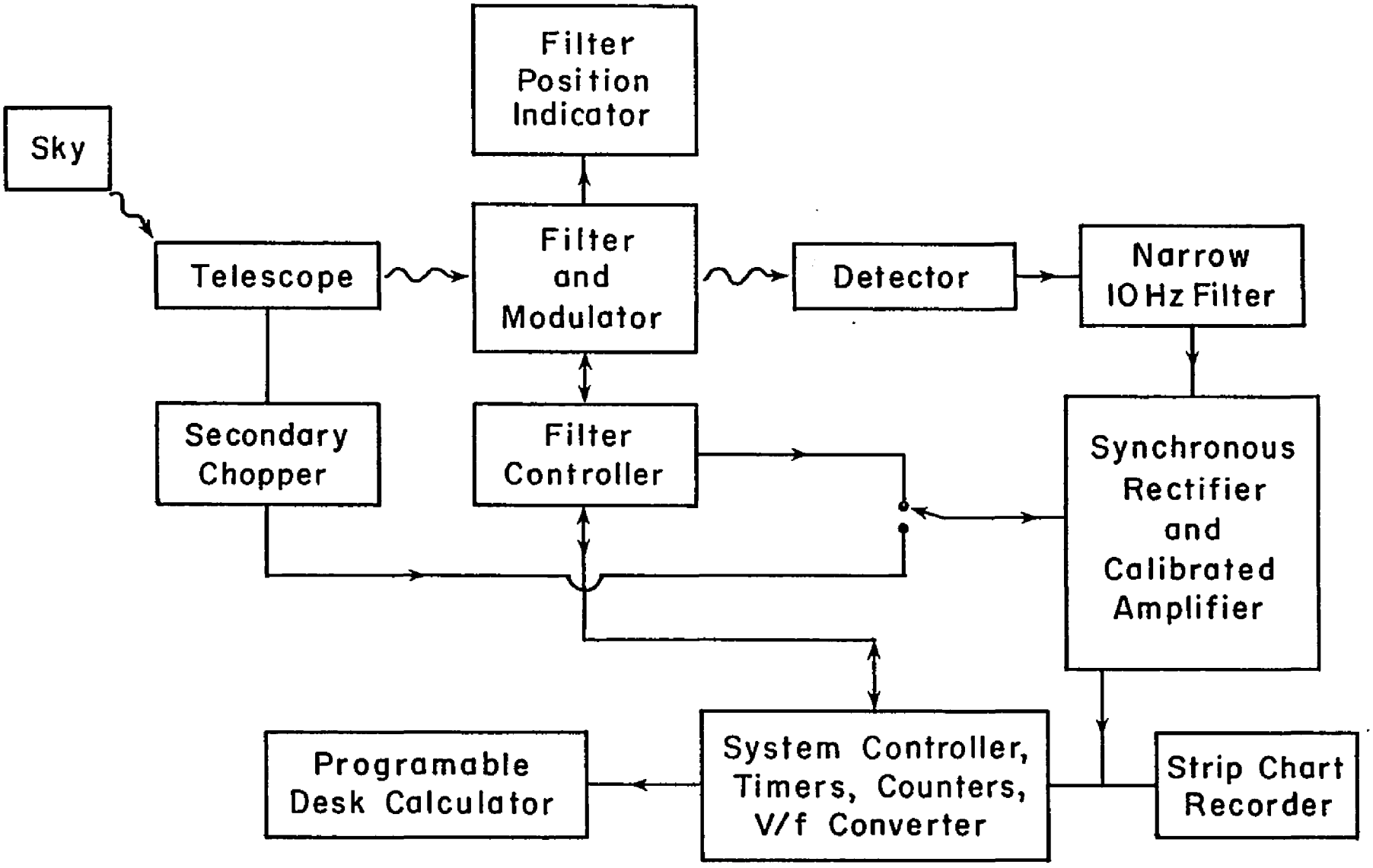

Figure 16. Block diagram of photometer system.

the synchronous rectifier which performed the actual comparison between the reference source (sky, toothed wheel, or adjacent spectral region) and the object of interest. The filtered DC output of the synchronous rectifier and calibrated amplifier was integrated by voltage to frequency converters and counters in the controller. Timers, also within the controller, could be adjusted to produce a suitable integration time. The integrated data was presented to the calculator which was typically programmed to print the raw numbers from the controller, subtract offsets and perform simple statistical calculations on the data in real time. The output of the synchronous rectifier was also displayed on a chart recorder which produced an additional record of the data, provided a check on the operation of the whole detection and data recording system and allowed convenient adjustments of the detector bias.

In actual operation at the telescope the toothed wheel chopper or the chopping secondary was used to produce spectral scans around the 1-0 S(1) line from 2.093 μ to 2.137 μ allowing measurement of both S(1) strength and continuum strength. Frequency chopping was used to automatically suppress continuum detection by first chopping between 2.122 μ 2.133 μ and then subtracting, with the calculator, the signal obtained by chopping between 2.104 μ and 2.122 μ. In this process the synchronous rectifier causes any S(1) signal to reverse sign between the two measurements while signal due to an underlying continuum retains the same sign and is subtracted out. In practice the frequency modulation technique does not completely cancel the continuum. This is because

the continuum of most stellar objects is not perfectly flat in the 2.1 μ region and the chopping was not done exactly symmetrically around 2.122 μ. The measured residual continuum strength was 0.7% of the continuum strength in the direction of a positive S(1) flux. This amount of error was not sufficient to produce false positive H_2 indications in any of the sources observed at the signal to noise levels achieved. Frequency chopping was used most often in the survey because it uses the telescope twice as efficiently as the toothed wheel measurements and does not depend on being able to chop to a section of sky with no H_2 emission as does the secondary chopper technique. Also some difficulty was encountered in using the secondary chopper at the large chopping distance needed.

The laboratory frequency calibration of the filter was verified during the first successful night of operation of the instrument by observing the Orion S(1) line in the spectral scanning mode. During the course of the observing program wavelength calibration was maintained to ±0.001 μ (one step of the stepper motor) by calibration of the filter position indicator before each telescope run, a recalibration of wavelength versus tilt angle with the FTS after several months of operation, and reverification of the position of the Orion S(1) line during each run when Orion was available. The filter position indicator was never off by more than one step after a run, the FTS recalibration showed no significant change in the filter and the Orion S(1) line always occurred in the same position to within one step. An error of one step could produce as much as 9% error in measured intensity due to

the steep sides of the filter passband. As an artifact of the mechanical part of the frequency chopper the filter could not be tilted quite far enough to completely eliminate S(1) radiation from the reference wavelength measurements. This resulted in a modulation efficiency (ratio of 1/2 the S(1) deflection in the frequency chopping mode to the S(1) deflection in the spectrum scanning mode) of 79% for the S(1) radiation. This problem was due to inadequate damping of the mechanical structure for large chop angles and could be eliminated by a more sophisticated chopping mechanism. In order to remove any baseline drift in the frequency chopping measurements an area of presumably blank sky was measured near each program object each night. Absolute flux calibration of the photometer was obtained by observing standard stars in the spectrum scanning mode and the modulation efficiency was measured by observing the Orion S(1) line in both the spectrum scanning mode and the frequency chopping mode. No correction for atmospheric extinction was applied to the data since the region of the S(1) line is quite free from atmospheric absorption. The absolute flux calibration accuracy is about 10%. When combined with other possible sources of error such as filter position inaccuracy the total error of the flux measurements is estimated to be about 15% (1 sigma).

CHAPTER 5

SURVEY OBSERVATIONS

The intent of the H_2 survey was to search for moderately low surface brightness H_2 emission sources among a wide variety of astronomical objects. At the outset of the survey observing program only two molecular hydrogen emission sources were known, Orion and NGC 7027. These sources belong to quite different classes of objects and represent a wide range in brightness. The average brightness of 7027 in a 36" beam is only 4% of the same average Orion brightness. On this basis it seemed worthwhile to examine a large variety of objects with some sacrifice in ultimate sensitivity in favor of increased sky coverage while maintaining a detection sensitivity at least below the brightness of NGC 7027. Following this philosophy the survey program objects were chosen to include several compact infra-red sources in molecular clouds because the Orion H_2 emission occurs near such an object. Planetary nebulae were observed to determine if any other than NGC 7027 showed H_2 emission. Supernova remnants were included because they should be sources of powerful shock waves which could excite nearby H_2. Dark clouds were observed because they probably contain considerable amounts of molecular hydrogen and would be interesting to compare to molecular clouds near HII regions and compact IR sources. External galaxies were included to see if enough molecular hydrogen would be excited in a whole galaxy to become visible over the other radiation

from the galaxy. Several T Tauri stars were selected, though only T Tauri itself was observed, because these stars are active and display a mass outflow which might excite H_2. Several miscellaneous objects such as CRL 437, CRL 961, OH 0739-14 and Sgr A were included, either because the object was expected to be near some H_2, as was the case with CRL 437 and Sgr A, or because the exact nature of the object was unknown and an H_2 observation would not only add to knowledge of H_2 sources, but might tell us something about the program object as well. The list of observed objects terminates where it does mainly because a decision was made to stop observing and begin writing this paper. I do not expect this list of objects to represent a complete sample of possible H_2 sources. Not only did I not thoroughly observe any one particular class of objects, but all the classes of objects in which H_2 emission might be expected are not even known. I may have been much too conservative in selecting miscellaneous objects for observation; no stars of moderate temperature were observed and no O or B stars isolated from molecular clouds were observed, for instance. We just do not yet know where to expect and where not to expect H_2 emission.

Search Method and Strategy

Many of the objects included in the survey were far too large to be surveyed completely. In the cases of molecular clouds with imbedded compact IR sources I began searching in a cross in RA and Dec, usually ±1' or 2' in size, centered on the IR source. If time or interest permitted, as in the case of M17, a filled box covering a large portion of the cloud, especially ionization fronts and bright, high density regions

from radio molecular maps, was surveyed. In other cases, where less time was used or available, linear scans across radio bright molecular concentrations and ionization fronts were made. If the molecular cloud was small either one point, as with K3-50, or a small cross, ±30", was observed. Dark clouds without IR objects, such as Barnard 35 and the "elephant trunks" in the Rosette nebula (NGC 2246), were observed with one or more linear scans arranged to include high density ridges (radio molecular features) and ionization fronts. Time was not available to survey significant portions of very large HII/molecular cloud complexes like W3. Supernova remnants were typically given a linear scan arranged to include the radio boundary of the SNR and any specially bright radio clumps. Planetary nebulae which were smaller than or on the order of the beam size were observed directly on the PN and typically in one or two other locations removed 25" or 30" from the center. Large planetaries (e.g., NGC 3587) were observed in several isolated points generally near the center and near one edge. Reference areas, near the program objects but chosen far enough away to be free (hopefully) of any possible H_2, were observed during every observation of a program object (with one or two exceptions noted in table 4) to remove the residual instrumental drifts as discussed in Chapter 4.

Signal to Noise Calculations

In the frequency chopping mode one observation of a point in the sky consisted of several, usually 10 to 15, individual measurements, usually 30 seconds integration time each, of the flux difference between the S(1) wavelength and the nearby continuum. An average

uncorrected S(1) flux, F, and error estimate, ε, were then produced for this observation via the formulae

$$\overline{F} = \frac{\sum_{n} F_i}{n} \tag{10}$$

and

$$\varepsilon = \sqrt{\frac{\sum_{n} (\overline{F} - F_i)^2}{n(n-1)}} \tag{11}$$

A series of such observations, including observations of reference areas, was then plotted against time and a zero S(1) flux reference was interpolated between the reference area values. The interpolated zero point was assumed to have the same error as the adjacent reference measurements. Since all observations in such a series were made with similar integration times the error derived as above for each observation was nearly equal for all observations in the series so no complicated procedure was used to combine the individual reference point errors to obtain the interpolated zero point error. The corrected S(1) flux was then obtained for each program observation by subtracting the interpolated zero point value from its corresponding program point value. The error in the corrected S(1) flux was then

$$\varepsilon_{corr} = \sqrt{\varepsilon^2 + \varepsilon_{zero}^2} \tag{12}$$

When a point in the sky was observed more than once (observations on several nights for instance) the several observations were

combined in a weighted average as

$$\bar{F} = \frac{\sum_{1}^{n} F_i/\epsilon_i^2}{\sum_{1}^{n} 1/\epsilon_i^2} \qquad (13)$$

with a resulting error

$$\epsilon = \sqrt{\frac{1}{\sum_{1}^{n} 1/\epsilon_i^2}} \qquad (14)$$

In the spectrum scanning mode spectra were co-added point by point using equation (10) and the uncertainty of the flux at each spectral point was determined with equation (11). If several averaged scans were combined, as in the case of the Sgr A observations, the averaged scans were weighted according to their signal to noise ratios and were co-added according to equations (13) and (14).

The complete list of surveyed objects and results appears in table 4. The 3 sigma detection level was typically maintained below 6×10^{-5} erg s^{-1} cm^{-2} sr^{-1}. NGC 7027's average brightness in 36" is 1.1×10^{-4} erg s^{-1} cm^{-2} sr^{-1}. The results of the survey fall into three categories: 1) upper limits which indicate no detected H_2 emission. 2) Possible detections which need confirmation. 3) Definite detections. One sigma errors are given for categories 2 and 3; however, when the error is less than 15% of the measured flux it should be taken

as an indication of the signal to noise ratio, not the accuracy of the measurement.

The observations from which table 4 is drawn were made with the 154 cm (61") telescope of the Catalina site of the University of Arizona's Lunar and Planetary Laboratory over the period 12 December 1976 to 22 November 1977.

Table 4

Summary of Observations

Object	Type[a]	Description of observation (epoch 1950)	Reference area	1-0 S(1) Flux (erg s^{-1} cm^{-2}) unless surface brightness is given	Category[b]
Barnard 35	DC	36" beam, ν chop, 2 linear scans (figure 17a)	2' N of BS 1987	scan 1 $<3.8\times10^{-12}$ at all points scan 2 $<1.2\times10^{-12}$ at all points	
Cas A 3C 461	SNR	36" beam, ν chop, 1 linear scan (figure 17b)	2' N of DM+58 2589	$<1.3\times10^{-12}$ at all points	
CRL 437	IR Nebula	30" beam, ν chop, ±60" cross in RA and Dec with 20" grid spacing, centered on $3^h3^m31\overset{s}{.}0$, +58°19'18" 260 s per point	1'30" N of DM+58 556	20"S $3.6\pm1.6\times10^{-12}$ 40"S $3.9\pm2.2\times10^{-12}$	2
CRL 961	IR Object	36" beam, ν chop, ±60" cross in RA and Dec with 30" spacing, 300s per point	1' S of DM+4 1327	$<6.8\times10^{-13}$ at all points	

Table 4. Summary of Observations (Continued)

Object	Type[a]	Description	Ref. Area	1-0 S(1) Flux	Category[b]
CRL 2688 "egg nebula"	pre PN?	36" beam, ν chop, 750's directly on CRL 2688	4' E of CRL 2688	$<7.6\times10^{-13}$[c]	
IC 418	PN	36" beam, ν chop, 2 measurements, one directly on IC 418 and one 25" N of the center, 600 s at each position	14!6 E of IC 418	$<1.2\times10^{-13}$ at either position	
IC 1396/ LkHα 349	MC	36" beam, ν chop, cross 5'N, 4'S, 5'30"E and 2'30"W with respect to LkHα 349. 900 s on eastern emission region, 180 s all other positions.	2' S of BS 8281	east $8.5\pm4\times10^{-5}$ erg $s^{-1}cm^{-2}sr^{-1}$ north $4.2\pm2\times10^{-5}$ erg $s^{-1}cm^{-2}sr^{-1}$ other points $<1.5\times10^{-12}$ erg $s^{-1}cm^{-2}$	3
IRC +10 216	IR star	36" beam, 5 point spectrum scan, 585 s total time	none	the measurement at 2.122 μ is $2.2\pm1.4\times10^{-23}$ erg $s^{-1}cm^{-2}Hz^{-1}$ below the interpolated continuum at 2.122 μ	

Table 4. Summary of Observations (Continued)

Object	Type[a]	Description	Ref. Area	1-0 S(1) Flux	Category[b]
K3 - 50	MC HII	36" beam, ν chop, 270 s each on K3-50, 25"W and 42"NE of K3-50, and ON-3(OH)	1' E of DM+33 3695	$<3.0\times10^{-12}$ at all points	
M1	SNR	36" beam, ν chop, 450 s on one point on the southern edge of the optical luminosity ($\alpha = 5^h31^m33\overset{s}{.}1$, $\delta = +21°56'58"$)	1' S of DM+21 902	$9.4\pm4.2\times10^{-13}$ erg $s^{-1}cm^{-2}$	2
M8	HII	36" beam, ν chop, 180 s on Herschel 36 ($18^h0^m36\overset{s}{.}4$, $-24°22'56"$)	55" E of 9 Sgr	$<1.2\times10^{-12}$ erg $s^{-1}cm^{-2}$	
M17	MC HII	36" beam, ν chop, see figure 17c	12' S of DM-16 4816	$<2.0\times10^{-12}$ at all points	
Mon R2	MC	30" beam, ν chop, 1140 s on IRS 3	4'15" W of DM-6 1412	$<1.7\times10^{-12}$	
NGC 2392	PN	30" beam, ν chop, 1260 s centered on 2392, 510 s 25" N of center	10' N of NGC 2392	center $<6\times10^{-13}$ 25" N $<1.4\times10^{-12}$	

Table 4. Summary of Observations (Continued)

Object	Type[a]	Description	Ref. Area	1-0 S(1) Flux	Category[b]
NGC 3242	PN	36" beam, ν chop, 570 s centered on 3242, 510 s at each of 25"S and 25'N of center	5' N of NGC 3242	center $1.1\pm0.2\times10^{-11}$ other points $<1.8\times10^{-12}$	2
NGC 3587	PN	30" beam, ν chop, 870 s at center of 3587 ($11^h11^m53\overset{s}{.}2$, +55°17'18")	4' E of center of NGC 3587	center $3.5\pm6\times10^{-12}$	2
		36" beam, ν chop, 990 s just within western edge of 3587 ($11^h11^m42\overset{s}{.}6$, +55 17'29") and 810 s just outside the optical edge ($11^h11^m43\overset{s}{.}5$, +55°18'43")	13' S of center of NGC 3587	west $1.8\pm4\times10^{-11}$	
NGC 4151	EG	30" beam, 5 point spectrum scan, 1800 s total time	none	$<7.5\times10^{-12}$	

Table 4. Summary of Observations (Continued)

Object	Type[a]	Description	Ref. Area	1-0 S(1) Flux	Category[b]
NGC 5195	EG	36" beam, ν chop, 5 point scan across 5195 with 33" separation. Start of scan $13^h27^m56\overset{s}{.}3$, +47°31'31", end of scan $13^h27^m43\overset{s}{.}1$, +47°31'27". 280 s at each point.	1' E of DM+47 2066	$<1.7\times10^{-12}$ at all points	
NGC 5236 (M 83)	EG	36" beam, ν chop, 1800 s centered on galaxy	30" N of NGC 5236	$<1.3\times10^{-12}$	
NGC 7027[d]	PN	36" beam, ν chop, 5040 s centered on 7027, 180 s each on 25"N and 25"S of center	4' E and 4' W of NGC 7027	center $2.48\pm.20\times10^{-12}$ other 1.8×10^{-12} points	3
NGC 7538 (N)-OH	MC	36" beam, ν chop, ±60" cross in RA and Dec centered on IRS 1 ($23^h11^m36\overset{s}{.}8$, +61°11'49"), 30" spacing. 720 s 30" N of IRS 1, 360 s on IRS 1, 180 s elsewhere	1'30" N or DM+60 2502	30" N or IRS 1 $2.2\pm0.6\times10^{-12}$ other $<1.8\times10^{-12}$	3

Table 4. Summary of Observations (Continued)

Object	Type[a]	Description	Ref. Area	1-0 S(1) Flux	Category[b]
OH 0739-14	OH IR	30" beam, 5 point spectrum scan, 2850 s total time	none	$<4.2\times10^{-12}$	
OMC-2	MC	30" beam, ν chop, see figure 20	45" S of θ^1C Ori	$<1.8\times10^{-12}$ at all points	
Orion H_2[d]	MC	30" beam, 5 point spectrum scan, 20" grid spacing, 150 s total time at each point, see figure 25	1' S of θ^1C Ori	see figure 25	3
R Mon	HII	30" beam, ν chop, 600 s on R Mon, 540 s on 20"S of R Mon	4' S of R Mon	R Mon $<3.0\times10^{-12}$ 20" S $2.1\pm0.7\times10^{-12}$	2
Rosette (NGC 2246)	DC HII	30" beam, ν chop, see figure 21	none	$<1.4\times10^{-12}$ at all points	
Sgr A	GC	36" beam, ν chop, 4620 s centered on IRS 7	various between 36" and 1'30" away from the Galactic Center	$<4.8\times10^{-13}$	
		36" beam, 5 point spectrum scan,	35" E and W of IRS 7		

Table 4. Summary of Observations (Continued)

Object	Type[a]	Description	Ref. Area	1-0 S(1) Flux	Category[b]
		centered on IRS-7, 7350 s total time			
Sgr B2	MC	36" beam, ν chop, see figure 22	1' S and 1' E of SAO 185759	$<1.5\times10^{-12}$ at all points	
SN +1572 (Tycho's) 3C10	SNR	36" beam, ν chop, see figure 23	2' N of DM+63 38	points 19 and 21 $1.4\pm0.8\times10^{-12}$ $<1.6\times10^{-12}$ at all other points	2
SN +1604 (Kepler's) 3C 358	SNR	36" beam, ν chop, see figure 24	4' N of DM-21 4638	$<2.8\times10^{-12}$ at all points except $3.5\pm1.0\times10^{-12}$ at points to the west	2
Sharpless 140/ Lynds 1204	MC	36" beam, ν chop, cross 1!5N, 1!5S, 2'E, 2!5W of CO hot spot ($22^h17^m35\overset{s}{.}7$, +63°04'02"), 30" spacing, 1320 s 40"N of CO, 180 s everywhere else	1' S of DM+62 2064	40" N of CO $8\pm3\times10^{-13}$ $<1.2\times10^{-12}$ at all other points	3
T Tauri	Star	30" beam, ν chop, 570 s on T Tau, 600 s 30"W of T Tau on NGC 1555	10' S of T Tau	$8.5\pm4.2\times10^{-12}$[e] on T Tau $<1.3\times10^{-12}$ 30"W	2

Table 4. Summary of Observations (Continued)

Object	Type[a]	Description	Ref. Area	1-0 S(1) Flux	Category[b]
W3 IRS 5	MC	30" beam, 5 point spectrum scan, covered a 2' square box centered on IRS 5 with a 30" grid spacing. 150 s total time at each point	none	$<6.2\times10^{-12}$ at all points	
W3(OH)	MC	36" beam, ν chop, see figure 26	2' E of SAO 12287	see figure 26	3

a. DC = dark cloud, EG = external galaxy, GC = Galactic Center, MC = molecular cloud, PN = planetary nebula, SNR = supernova remnant

b. no entry means category 1: no detected 1-0 S(1) emission, 3 σ upper limit given

c. Detected by Beckwith, Persson and Gatley (1978) at $5 \pm 2 \times 10^{-13}$ erg s^{-1} cm^{-2}

d. previously known H_2 source

e. Detected by Beckwith, Gatley, Matthews and Neugebauer (1978) at $5.7 \pm 1.0 \times 10^{-13}$ erg s^{-1} cm^{-2}

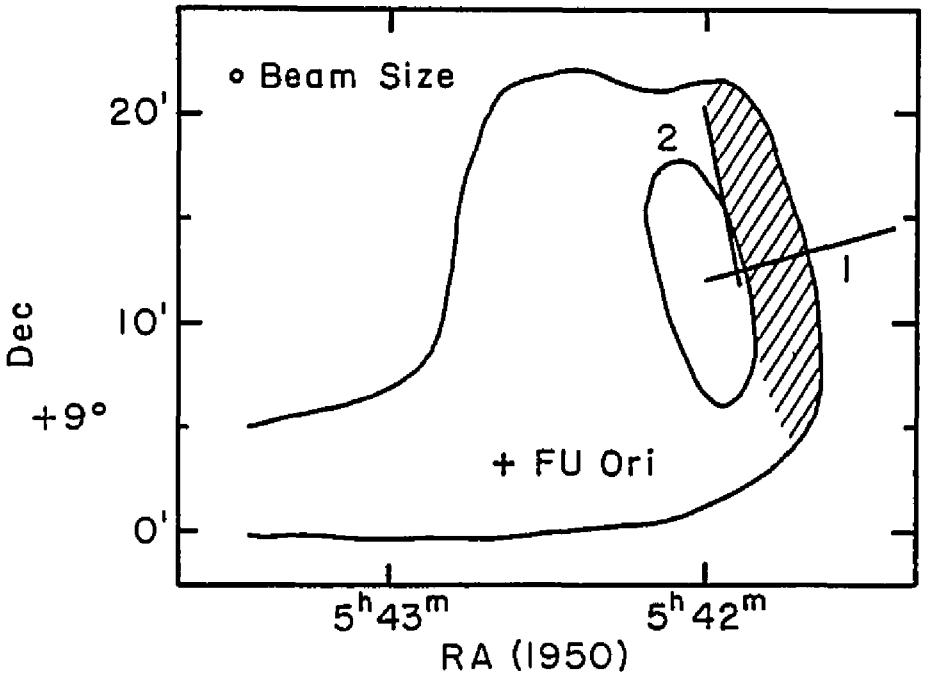

Figure 17. Barnard 35. -- Solid contours are the outer limits of the CO cloud and the approximate area of maximum CO emission. Cross hatching is the bright rim of Barnard 35. Survey scans had 27" point spacing with 150s integration time per point. Map adapted from Lada and Black (1976).

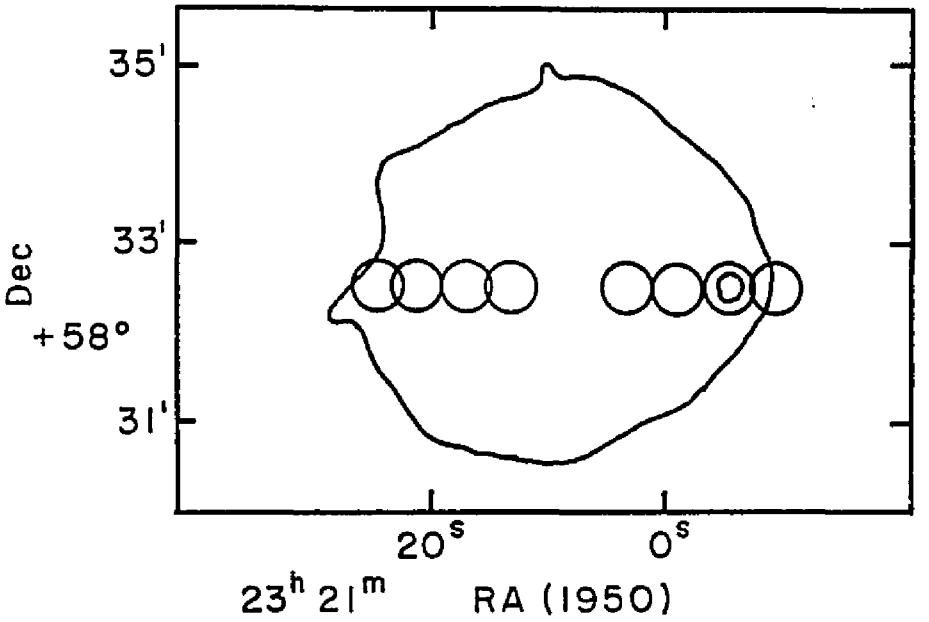

Figure 18. Cas A. -- Solid contours are the outer limit of strong 1.4 GHz emission and the 1.4 GHz "hot spot". Circles represent the actual beam areas on the sky. 180s integration time per point. Map adapted from Ryle, Elsmore and Neville (1965).

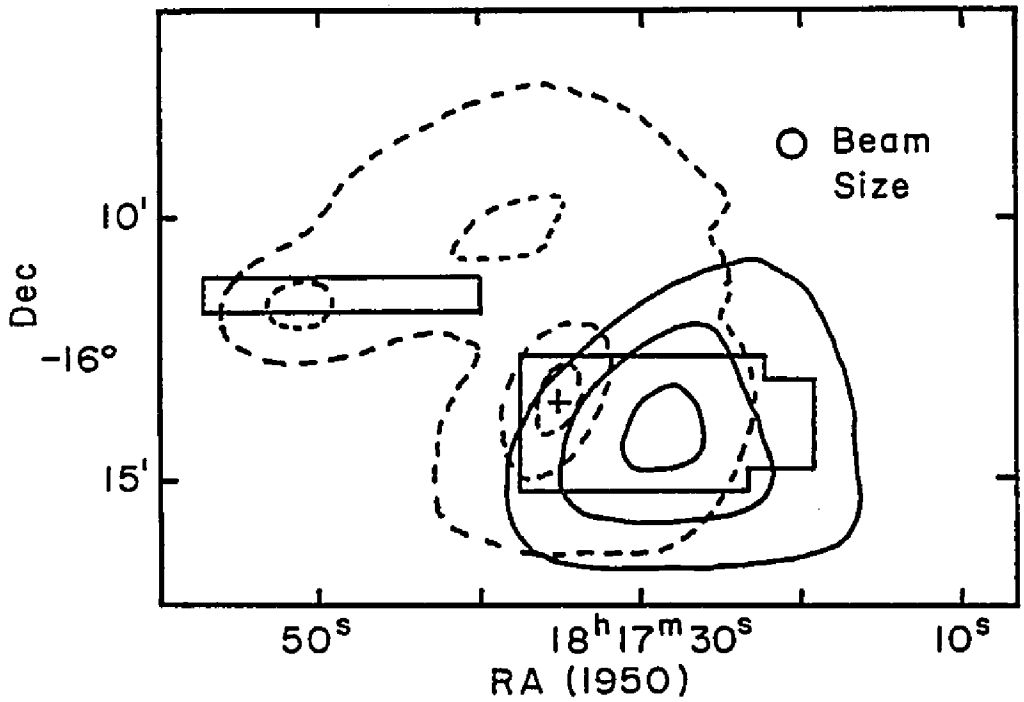

Figure 19. M17.-- Solid contours are CO intensity from Lada, Dickinson, and Penfield (1974) and dashed contours are 21 μ intensity from Lemke and Low (1972). The cross is BD -16 4816. The solid boxes were completely scanned with a grid spacing of 30" and 210s integration time per point.

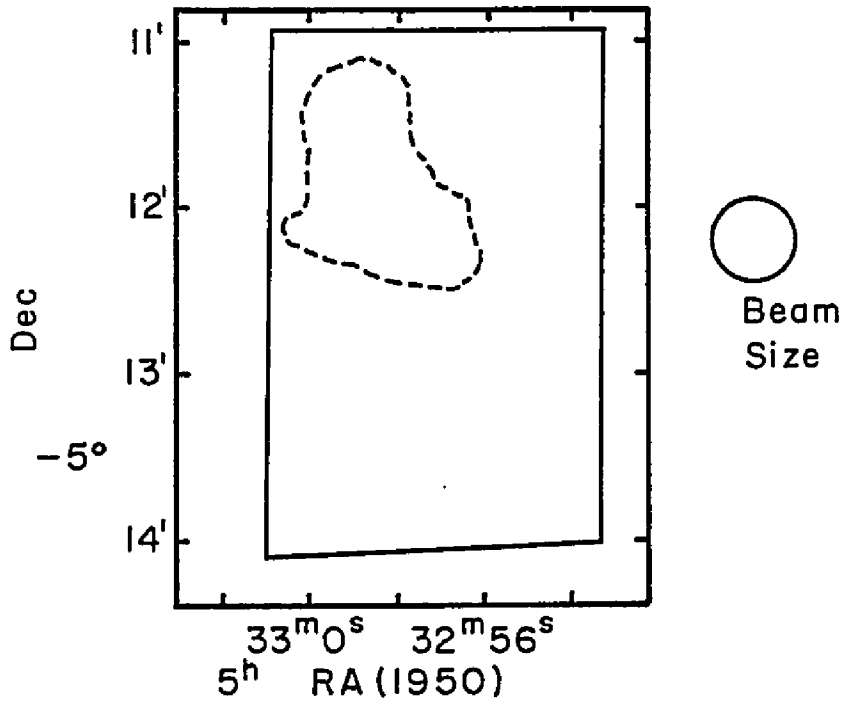

Figure 20. OMC-2. -- The dashed contour surrounds the group of IR sources described in Gatley et al. (1974). The solid box was completely surveyed with a grid spacing of 30" and 120s integration time per point.

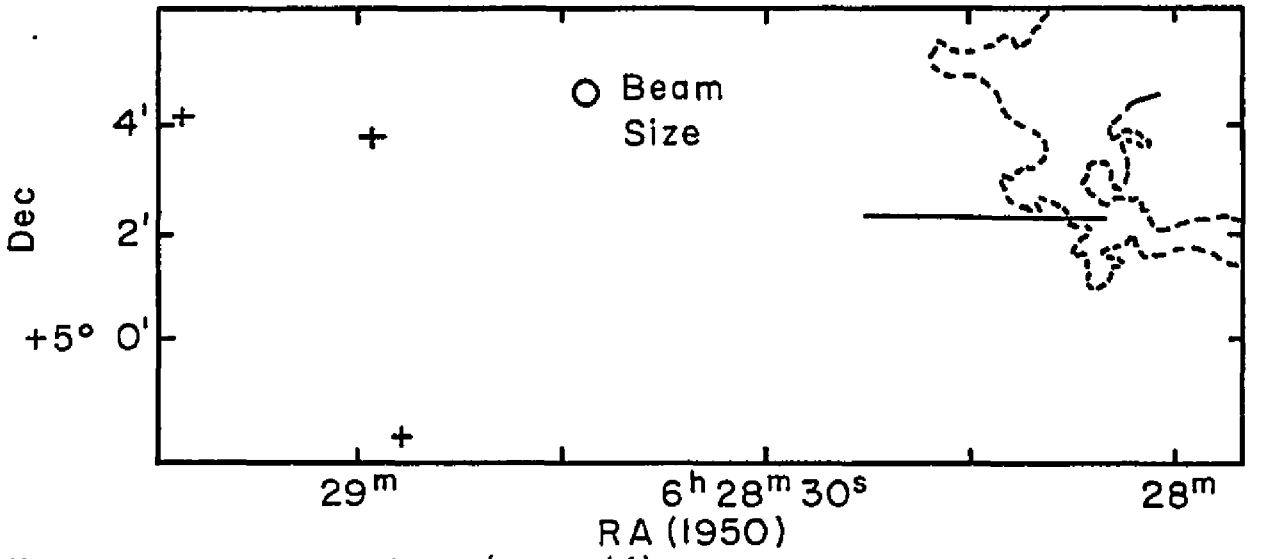

Figure 21. Rosette nebula (NGC 2246). -- Crosses mark the positions of the central OB stars of NGC 2244 and the dashed contour outlines the dark globule structure included in the survey scan. The point spacing in the scan was 30" with 220s integration time per point.

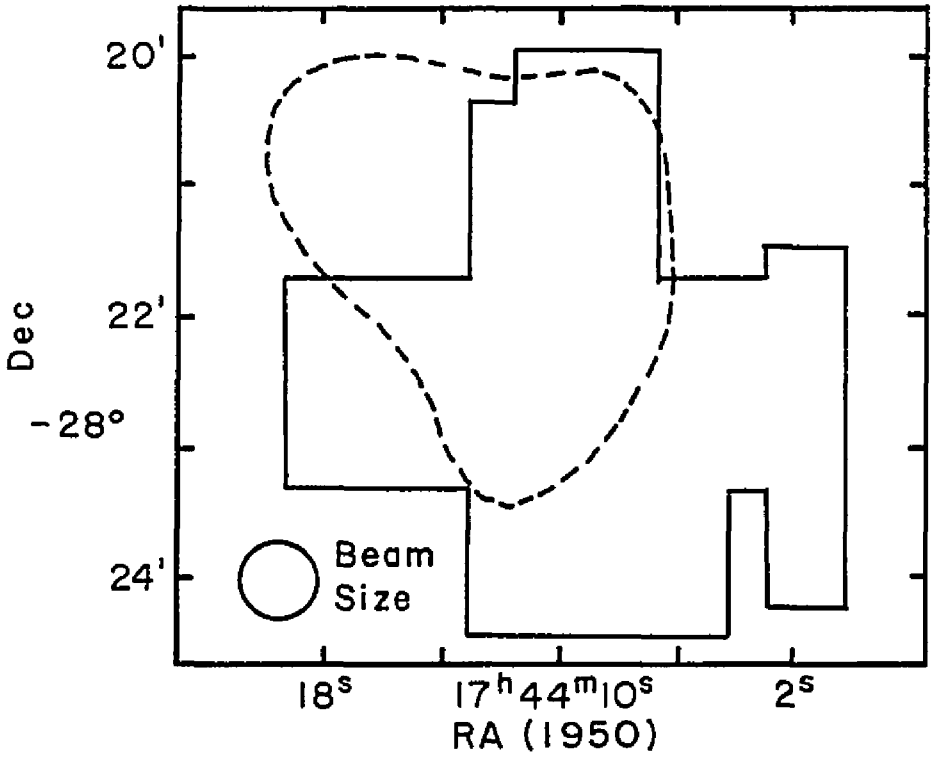

Figure 22. Sgr B2. -- The dashed contour is the 10% continuum level as shown in Martin and Downes (1972). The solid line outlines the area surveyed with a 30" grid spacing and 180s integration time per point. The area in the center of the general cross shape was observed twice.

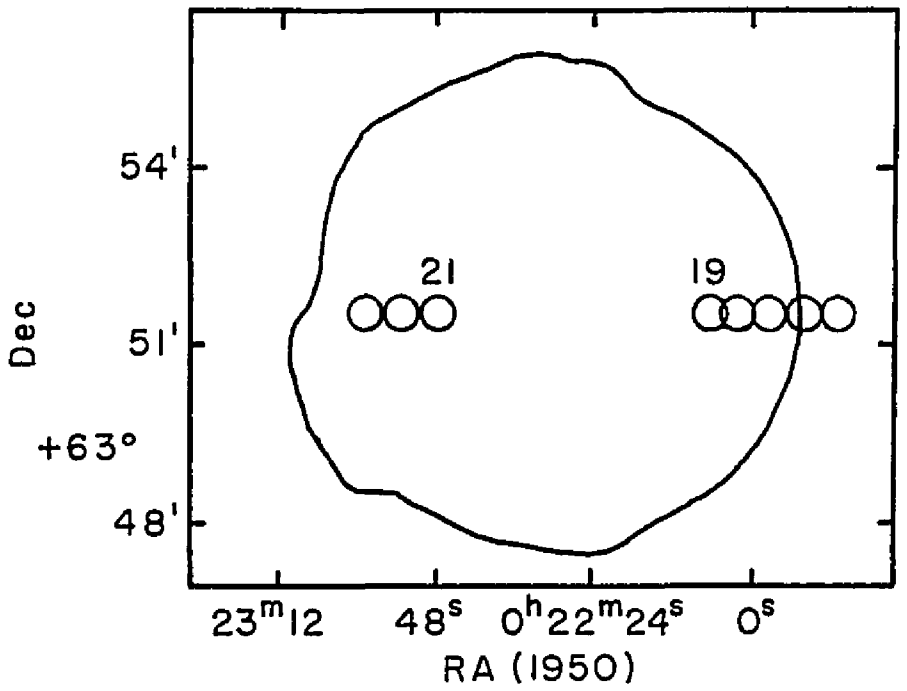

Figure 23. SN +1572. -- The solid contour is the outer limit of the 1.4 GHz continuum emission as shown in Strom and Duin (1973). The circles represent the actual beam areas. 270s integration time per point.

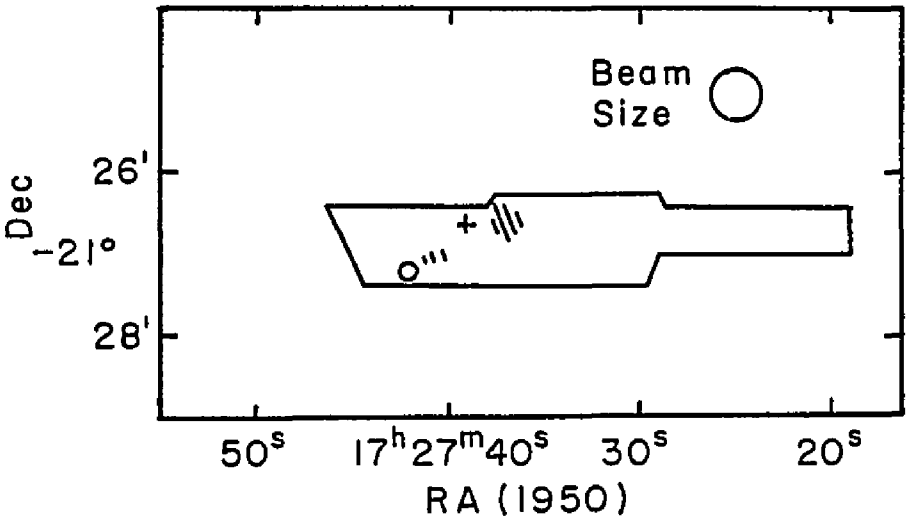

Figure 24. SN +1604. -- The cross is the position of the nova, the circle the center of 3C10. The cross hatching is nebulosity and the solid box was surveyed with 30" grid spacing and 220s integration time per point. The possible H_2 emission occurred in the western extention of the box. The map was adapted from Minkowski (1968).

CHAPTER 6

H_2 NEAR HII

Before this survey the Orion H_2 emission was the only known molecular hydrogen source near a large HII region or molecular cloud. Three of the new H_2 sources are in large molecular clouds near HII regions. These sources, Sharpless 140, W3(OH) and NGC 7538 (N)-OH have much in common with the Orion nebula and, with Orion, form one class of H_2 emission sources.

Orion

The Orion H_2 emission occurs near the apparent heart of the Orion molecular cloud about 60" N and 40" W of θ^1C Ori. Figure 25 is a low resolution map of the H_2 emission produced from the survey observations. The outer contour of this map encloses two IR point sources (BN and IRS-2), an extended far infra-red emission region (the KL nebula), several H_2O maser emissions and part of an ionization ridge between θ^1C and the molecular cloud (Hollenbach and Shull, 1977). Ionized hydrogen is known to be present in a small region around the BN object (Grasdalen, 1976; Joyce, Simon and Simon, 1978; and Hall, Kleinmann, Ridgway and Gillett, 1978). A region of ^{12}CO emission showing very extended line wings is also centered near the H_2 emission. Beckwith, Persson, Neugebauer and Becklin (1978) have shown the H_2 emission to be concentrated in several bright emission knots. This survey did not include a

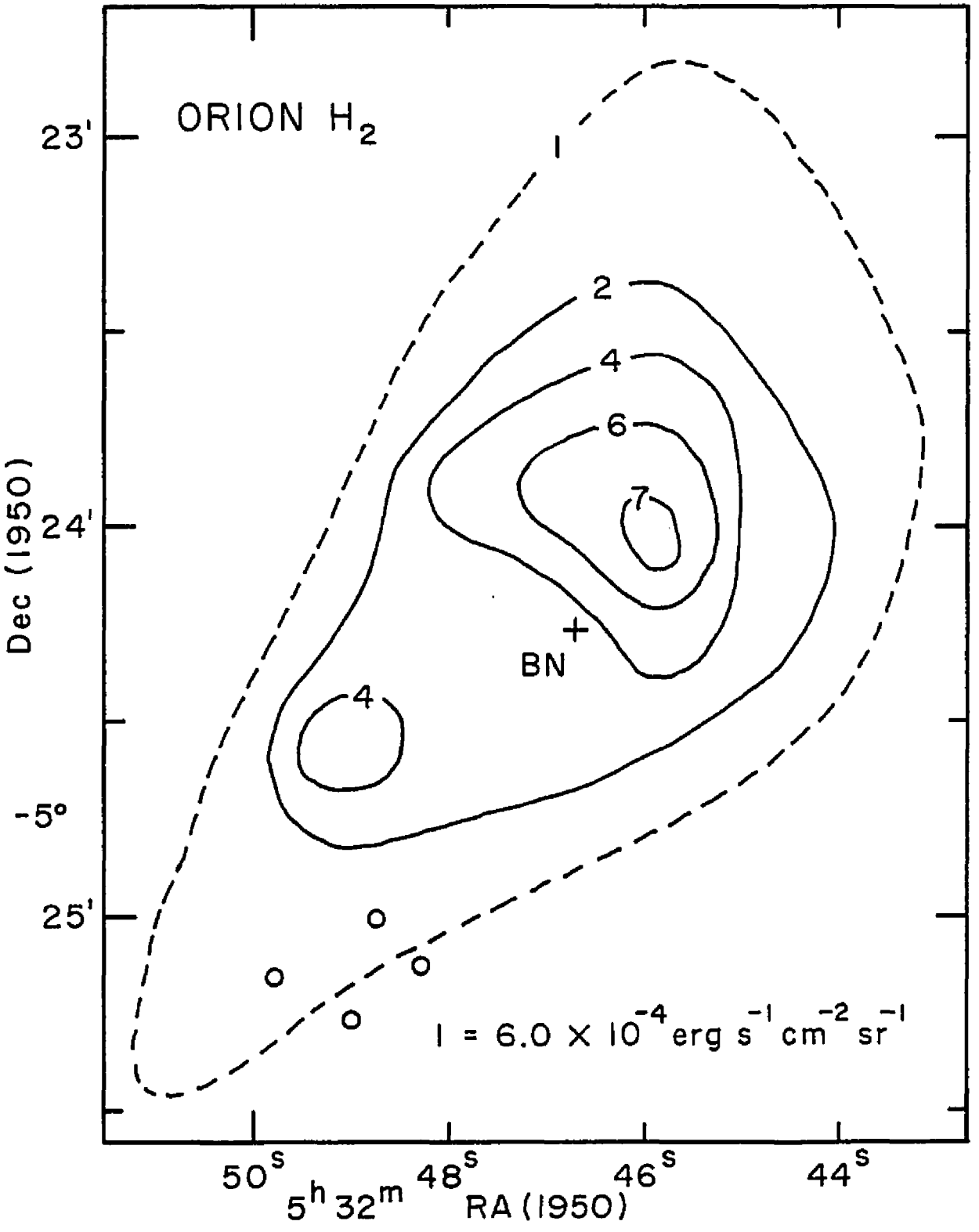

Figure 25. Map of the Orion H_2 emission. -- The signal to noise at the outer contour is about 2 to 1. The beam size was 30". The small circles represent the trapezium stars.

detailed examination of the Orion H_2 due to lack of time and because Beckwith, Persson, Neugebauer and Becklin (1978) had made detailed observations of the region. The survey observations do, however, extend the known limits of the H_2 emission to much lower surface brightness and larger area. Our map should be considered incomplete because it stops short of following the H_2 emission into the noise toward the west and because it was produced very early in our program when the instrument was operating at less than its maximum sensitivity. The sensitivity was later improved by a factor of six but only one linear scan was then made across the Orion H_2 emission to verify the earlier observations. A map quite similar to figure 25 was recently published by Beckwith, Persson, Neugebauer and Becklin (1978). Tables 5 and 6 contain entries for Orion for comparison with the new H_2 sources.

S140

The Sharpless 140 molecular cloud appears as a dark cloud (also known as Lynds 1204) at the northeast boundary of the HII region Sharpless 140. A considerable number of observations have been recently made of S140 because its simple structure lends itself to direct, simplified interpretation. Lynds 1204 contains a 2 μ infra-red source coincident with a strong far IR source and near an H_2O maser and a peak in the ^{12}CO emission intensity. There is also a weak radio continuum source in the near vicinity. Radio emissions from formaldehyde and HCN have also been observed from the region of the CO peak. This group of sources is located 1/2 to 1 arc minute behind the ionization front between S140 and L1204. More detailed descriptions of the region may

Table 5

Derived Parameters of H_2 Sources

Source	Distance	Size Sr	Average Brightness erg $cm^{-2}S^{-1}Sr^{-1}$	$N(H_2)$ cm^{-2} 2000K	$M(H_2)$ (2000K) $M_\odot$	$L_\odot$ Luminosity S(1)	$L_\odot$ Luminosity Total (2000K)
NGC 7538 (N)-OH	3.5 kpc	$\leq 5.9\times10^{-9}$†	$\geq 3.7\times10^{-4}$	$\geq 1.1\times10^{18}$	2.7×10^{-3}	.83	5.9
S140	910 pc	2×10^{-7}††	3.5×10^{-5}	9.9×10^{16}	2.8×10^{-4}	.17	1.2
W3(OH) E	3 kpc	9.6×10^{-8}	5.7×10^{-5}	1.7×10^{17}	5.1×10^{-3}	3.3	23
W		9.6×10^{-8}	6.8×10^{-5}	2.0×10^{17}			
LkHα 349	1 kpc	7×10^{-8}*	8.5×10^{-5}	2.5×10^{17}	2.8×10^{-4}	.18	1.3
Orion all	450 pc	1.1×10^{-7}	2.4×10^{-3}	7.0×10^{18}	2.5×10^{-3}	1.6	11.6
Orion central 35"		2.2×10^{-8}	3.6×10^{-3}	1.1×10^{19}			

*Since this was only 1 scan across the region the actual size could conceivably be 3-4 times larger.

†The whole region of NGC 7538 (N)-OH is only 18" in diameter, only half the diameter of the survey beam. The entries for 7538 were calculated with 18" as an upper limit to the size.

††The north-south extent of S140 H_2 is $\sim$1.'5. The east-west extent was not determined. The table entries are calculated assuming an east-west extent of 1.'5.

Table 6

Calculated Thickness of H_2 Emissions

Source	Average Thickness ($p \geq 10^5 cm^{-3}$)	Size	Thickness Ratio
NGC 7538 (N)-OH	$\leq 1.7 \times 10^{13}$cm	$< 9.4 \times 10^{17}$cm	$< 9 \times 10^4$
S140	$\leq 1 \times 10^{12}$cm	1.4×10^{18}cm	$\sim 10^6$
W3(OH)	$\leq 2 \times 10^{12}$cm	4.2×10^{18}cm	$\sim 10^6$
LkHα 349	$\leq 2.5 \times 10^{12}$cm	1.3×10^{18}cm	$\sim 5 \times 10^5$
Orion	$\leq 7.0 \times 10^{13}$	9.1×10^{17}cm	1.3×10^4

be found in papers by Knapp et al. (1976), Blair et al. (1978) and Harvey, Campbell and Hoffman (1978). The center of the H_2 emission region is approximately $\alpha = 22^h17^m35^s.6$, $\delta = +63°4'39''$ (1950), 50" N and 40" W of the near infra-red point source. This position is near the ^{12}CO peak but our mapping was not done in sufficient detail to determine the exact degree of coincidence of the H_2 and CO emissions. The H_2 emission is extended at least on the order of 1.5'.

In the absence of knowledge of the emission in H_2 lines other than S(1) it is probably not unreasonable to presume that the excitation conditions of the emitting molecular hydrogen in S140 are similar to those of the H_2 in Orion. The volume density of molecular hydrogen near the CO peak and the IR source was determined from formaldehyde observations to be about 3×10^5 cm^{-3} in the region of the H_2 emission in S140 (Blair et al., 1978). This is sufficient to thermalize the vibration-rotation energy levels of H_2 in the wake of a shock and is near the density of H_2 determined for the Orion molecular cloud. The association of the ionization front, CO emission, IR point source and maser is likewise similar to Orion. Table 5 lists several derived parameters of the H_2 emission region based on the theoretical result that the observed excitation temperature of the H_2 will always be near 2000K. The column density in table 5 and the volume density given above yield an average thickness (table 6) of the emitting region along the line of sight of 10^{12} cm, assuming 2000K. This is about 10^6 times smaller than the extent of the region perpendicular to the line of sight

and we conclude that the H_2 is confined to thin sheets, similar to the Orion source. The exact thickness derived for the emitting region depends, of course, on the assumed temperature of the H_2. Temperatures lower than 2000K would yield thicker sheets; 1600K, the lowest temperature expected by theory from shock heating, would produce sheets 1.8 times thicker.

W3(OH)

The region of W3(OH), located on the southeastern edge of the HII region W3 (IC 1795), contains two compact infra-red sources, a compact radio continuum source, an H_2O maser and an OH maser within an area 1 arc minute across (see figure 26). More detailed information may be found in papers by Mezger et al. (1967), Wynn-Williams (1971) and Wynn-Williams, Becklin and Neugebauer (1972). The position and extent of the H_2 emission is also shown in figure 26. Table 5 again lists derived parameters for W3(OH) H_2 under the assumption of thermalization to 2000K and again the thickness of the H_2 emission region is very small compared to its perpendicular extent (table 6).

NGC 7538 (N)-OH

The region of NGC 7538 (N)-OH lies on the southern edge of the visible HII region NGC 7538 and contains three compact radio continuum sources, an OH maser, molecular line emission sources and three IR sources coincident with the radio continuum sources. More details may be found in Martin (1973) and Wynn-Williams, Becklin and Neugebauer (1974). The H_2 emission was detected with our 36" beam centered 30" N

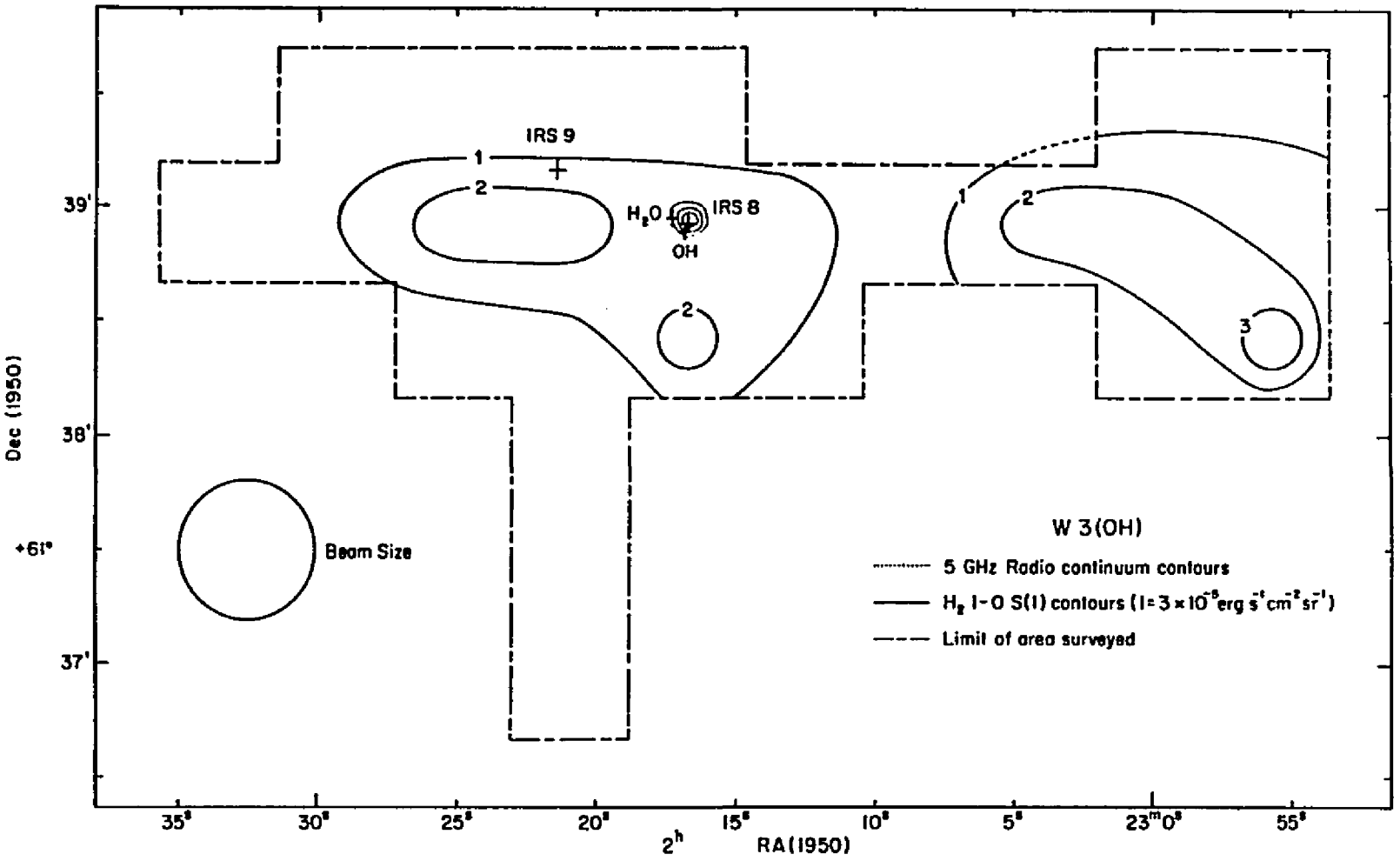

Figure 26. Map of the W3(OH) H_2 emission. -- The positions of the IR and molecular sources and the 5GHz continuum contours were obtained from Wynn-Williams (1971) and Wynn-Williams, Becklin, and Neugebauer (1972).

of IRS 1 (see Wynn-Williams, Becklin and Neugebauer, (1974). No other beam position in a ±1' cross centered on IRS 1 showed any H_2 emission to a 3 sigma upper limit of 2×10^{-12} erg s^{-1} cm^{-2}. The entire region of NGC 7538 (N)-OH is only 18" in diameter so it is impossible to determine the size of the H_2 emission from the present data. The entries in table 5 reflect the assumption that the emission is extended on the order of 18" as well as the H_2 being thermalized at 2000K. If the H_2 source is smaller than 18" the column density increases. However, assuming a space density of $\sim 10^5$ cm^{-3} for H_2 within the source, the emission must still originate in a thin sheet (thickness ratio >10) unless the true size of the emitting region is less than 1". Dr. Phillip Solomon originally suggested NGC 7538 as a likely H_2 source.

As mentioned before, Orion, S140, W3(OH) and NGC 7538 (N)-OH H_2 sources are all situated in dense molecular clouds near compact infra-red sources, OH and H_2O masers and CO and other molecular line sources. All also have indications of small, young HII regions near or around the compact IR sources; S140, NGC 7538 (N)-OH and W3(OH) have radio continuum sources and the BN object in Orion is known to show atomic hydrogen Brackett α emission, probably indicating the presence of either a compact HII region or an accretion shock front surrounding a proto stellar object at the center of BN (Grasdalen, 1976; Joyce, Simon and Simon, 1978). These features are characteristic of active or very recent star formation. In the case of NGC 7538 (N)-OH, Martin (1973) estimates an age of 3000 years for one of the IR sources and Hall, Kleinmann, Ridgway and Gillett (1978) suggests that BN

represents the earliest stage of stellar evolution yet clearly identified. H_2 emission from these very young regions should be contrasted with the absence of detectable H_2 emission from the molecular cloud in M17, an older region where star formation processes are apparently no longer active. This suggests that whatever process excites molecular hydrogen in large molecular clouds is most active near the sites of most recent star formation. The survey observations of W3 IRS-5, K3-50, Mon R2 and M8, regions relevant to this discussion, were not extensive enough to include in this argument.

Since only the 1-0 S(1) transition has been observed in the new H_2 sources, my interpretation of emission from thin sheets of gas thermalized at 2000K is not the only possible one. Retaining for a moment the assumption of thermalization, the survey's spatial resolution is not sufficient to detect any small scale clumping or filamentary structure in the excited H_2. A filling factor of approximately 1% with long filamentary emission regions would result in roughly cylindrical filaments which could conceivably be scattered throughout a volume of space with a depth comparable to the observed projected extent of the H_2 emission. This would not affect the assumption of optical thinness. Values of the column density $\sim 4 \times 10^{24}$ cm^{-2} are needed to give an optical depth of one in the S(1) line, assuming a square line profile with a doppler width of 3.4 km s^{-1} appropriate for H_2 at 2000K. With the typical observed average column density of 10^{17} cm^{-2} a filling factor of 10^{-8} is needed to make S(1) optically thick. Other perforated or disconnected geometries are also possible. A considerably lower

temperature than the assumed 2000K would also lead to a much thicker emitting region. Temperatures of 400 to 500K would yield thickness ratios of 1 to 10 in the newly observed H_2 emissions. Although such low temperatures are not eliminated by these observations they are not consistent with the theoretical results for shock heating. (To be sure, there is H_2 at 400-500K in the shock heated model but the hotter H_2 swamps its emission.) It is also possible that the space density of the H_2 is less than 10^5 cm^{-3} in the regions of H_2 emission. This would affect the thin sheet interpretation both by making the sheets thicker in inverse proportion to the H_2 density and by invalidating the assumption of thermalization of the H_2 by collisions which allows the simple calculation of column densities.

I have also evaluated the possible excitation of the observed H_2 due to near ultra-violet fluorescence, the best understood alternative to thermal excitation. I compared the total possible 1-0 S(1) emission due to nearby sources of photons in the range 1100-912A with the observed S(1) luminosities of the new sources assuming no extinction of the S(1) radiation by intervening material. These results are summarized in table 7. In the case of W3(OH) I obtained a probable spectral type for the IR source near the H_2 emission by comparing the excitation parameter of the compact radio source (Wynn-Williams, 1971) with the calculations of the properties of HII regions by Prentiss and ter Harr (1969) and Rubin (1968). The spectral type of the brightest IR source in NGC 7538 (N)-OH was derived from the 1-25 μ luminosity of the IR source and the calculations of Panagia (1973), assuming that the

Table 7

Source Parameters for UV Fluorescence Mechanism

Source	S(1) Luminosity ($L_\odot$)	Angle Subtended by H_2 Source ($\omega/4\pi$)	Stellar Luminosity $912<\lambda<1100$Å	Required Stellar Luminosity	Calculated Stellar Luminosity	Calculated Stellar Type
S140[†]	1.7×10^{-1}	.125	6% 13%	$9.0\times10^{4}L_\odot$ 4.4×10^{4}	$8.9\times10^{3}L_\odot$ 2.4×10^{4}	B1V[††] B0 ZAMS
LkHα 349	1.8×10^{-1}	3.5×10^{-4}	14% 13%	1.6×10^{7} 1.7×10^{7}	6.6×10^{5} 3.6×10^{5}	06I [Of6 06V Observed]
W3(OH)	3.3	1.43×10^{-2}	14%	7.1×10^{6}	6.6×10^{5}	O6
NGC 7538 (N)-OH	8.3×10^{-1}	6.25×10^{-2}	13% 14%	4.4×10^{5} 4.1×10^{5}	3.8×10^{4} 6.6×10^{4}	O9.5 ZAMS O9.5V

[†]Entries for S140 calculated assuming an east-west extent of 1'.5. If the actual size is smaller the required stellar luminosity will be proportionately closer to the calculated stellar luminosity.

[††]Spectral types estimated by Knapp et al. (1976) and Harvey, Campbell and Hoffmann (1978).

IR star is either a zero age main sequence or luminosity class V star. The conversion efficiency of absorbed UV photons to S(1) photons was taken to be 2% from Black and Dalgarno (1976) and, following Hollenbach and Shull (1977), the H_2 was assumed to absorb 25% of the incident NUV photons with dust absorbing the rest. The distance between the ionizing source and the excited H_2 was taken to be their projected distance separation on the sky. Table 7 indicates that all the UV sources with the possible exception of S140 IR are too dim by a factor of at least 7 to produce the observed S(1) fluxes. S140 IR is only too dim by a factor of 2 which, due to the approximate nature of this calculation and the possibility that the population of the upper level of the 1-0 S(1) transition may be enhanced by some process not accounted for, is not large enough to exclude the possibility of NUV fluorescence as the main excitation process for H_2 in S140 so long as the S(1) radiation suffers no extinction. On the other hand the 10 μ silicate absorption feature of S140 IR has the same depth as in the BN object (Blair et al., 1978 and Harvey, Campbell and Hoffmann, 1978) which indicates a 2 μ extinction of at least three magnitudes to the IR source. If the H_2 emission originates from a similar depth within the cloud the possibility of NUV excitation is unlikely.

Since all the new H_2 sources are many times fainter than the Orion source it is of interest to determine if the new sources have intrinsically lower surface brightness or if there are large amounts of interstellar matter obscuring the new sources. Unfortunately the survey measurement of the 1-0 S(1) strength alone cannot shed much light on

this question but a consistency check can be made with theoretical calculations. The results of Kwan (1977) relating the expected surface brightness of the 1-0 S(1) radiation to shock velocity and preshock H_2 density are reproduced in figure 27. As can be seen the average surface brightness of Orion ($\sim 3 \times 10^{-3}$ erg s^{-1} cm^{-2} sr^{-1}) indicates a preshock hydrogen density greater than 10^5 cm^{-3} for all shock velocities between 5 and 25 km s^{-1}. This density is high enough to produce thermalization of the vibrational and rotational energy levels which produce the observed 2 μ radiation. The new sources all have surface brightnesses around 7×10^{-5} erg s^{-1} cm^{-2} sr^{-1}, a value lower than the range displayed in figure 27. A naive extrapolation of Kwan's results associates a preshock density much less than 10^5 cm^{-3} with a surface brightness of 7×10^{-5} erg s^{-1} cm^{-2} sr^{-1}, at least for shock velocities between 10 and 25 km s^{-1}. This extrapolation is probably not valid since it leads to preshock densities too small for thermalization of the vibration-rotation levels of H_2 to occur; however, it does indicate a possible discrepancy between the characteristics of the new H_2 sources and present shock heating models. If the new H_2 sources suffer more extinction than the Orion source this problem would be removed and the shock heating model could be more comfortably assumed for the new sources. An extinction of ~ 4 magnitudes at the S(1) line would be needed to bring the unextinguished surface brightness of the new sources up to a level consistent with a preshock density of 3×10^5 cm^{-3}. Values of 2 μ extinction at least as high as four magnitudes are reasonable to expect for sources deep within dense molecular clouds.

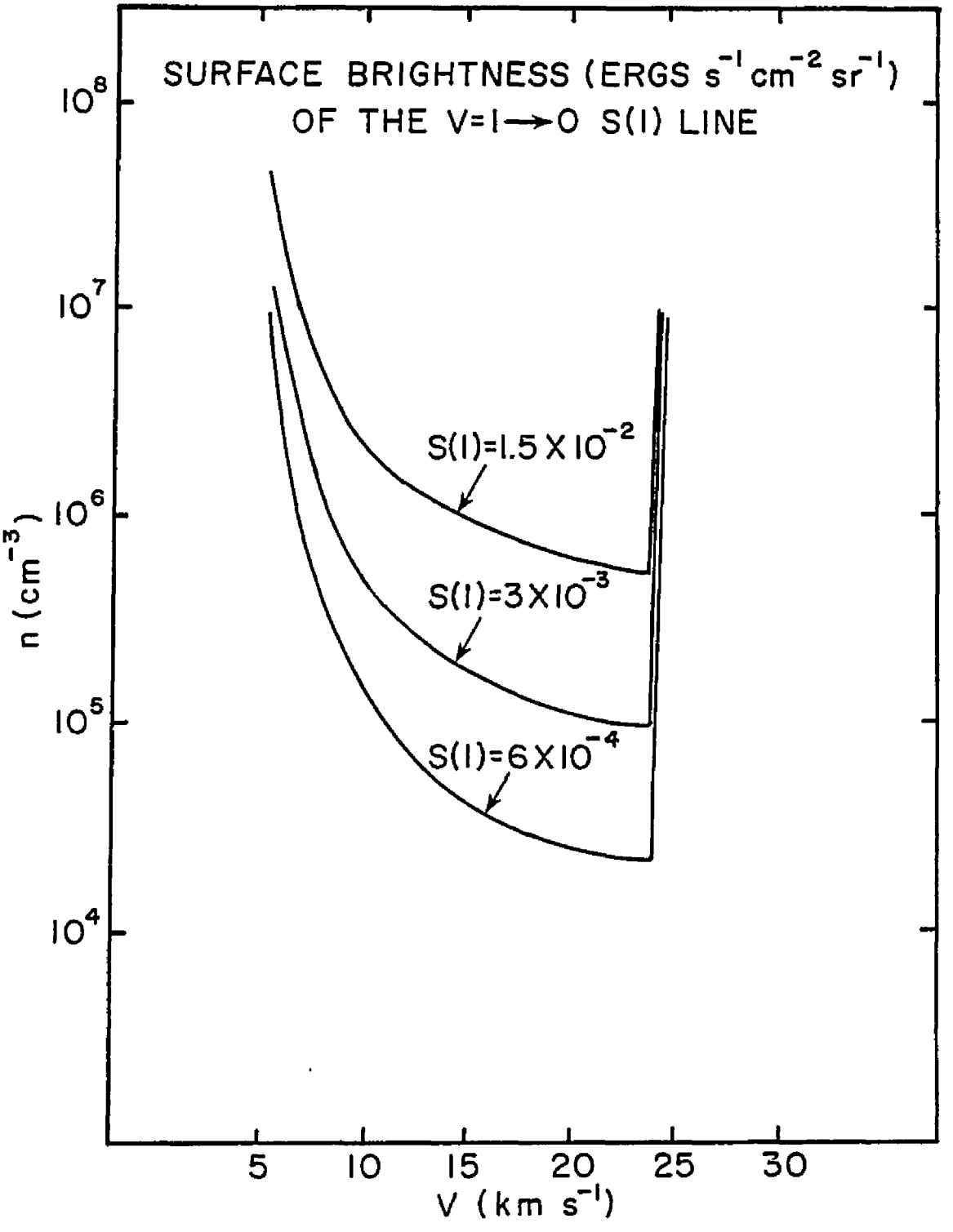

Figure 27. Surface brightness of 1-0 S(1) from shock heating calculations. -- This figure was adapted from Kwan (1977).

Future observations of more H_2 lines in these new sources should reveal whether the new H_2 is thermalized or not. If the new H_2 is thermalized, extinction by intervening material will produce characteristic differential extinction among the 2 μ H_2 lines. The absence of such differential extinction in an apparently thermal spectrum would indicate the low average surface brightness is due to a low filling factor for the excited H_2.

CHAPTER 7

OTHER H_2 SOURCES

A wide variety of astronomical objects have now been examined for 2 μ H_2 emission. Four classes of objects other than dense molecular clouds near HII regions have at least one member which emits 2 μ H_2 line radiation. These are discussed below. The bulk of the objects examined show no H_2 emission at the current level of sensitivity. There are, however, tantalizing hints that an improvement in sensitivity of a factor of 3 to 10 would reveal a much larger number of molecular hydrogen emission objects.

LkHα 349

This emission line star lies at the apparent center of a bright rimmed cloud of about 130" radius at the end of an "elephant trunk" structure in the HII region IC 1396. Descriptions and photographs of the region may be found in Dibai and Esipov (1968) and in Loren, Peters, and Vanden Bout (1975). The H_2 emission is from an extended region 30" E to 1'30" E of the emission star ($\alpha = 21^h35^m21^s.9$, $\delta = +57°17'35"$, 1950 at the center of detected H_2 regions). This is within the dark cloud about half way between the star and the bright rim in the direction of the ionizing source of IC 1396. The extent of the H_2 emission in declination was not determined except that some emission was seen 1'30" N of LkHα 349 at $\alpha = 21^h35^m17^s.9$, $\delta = +57°19'05"$. Loren, Peters

and Vanden Bout (1975) derive a volume density of $\sim 10^5$ cm^{-3} in the dark cloud and have detected emission lines of CO over a large part of the cloud and elephant trunk. Radio lines of SO, HCN and CS have been detected at the peak of the CO emission. This high density again invites the assumption of shock excitation of the H_2 and appropriate entries have been made in table 5 for LkHα 349. As in the other sources, this assumption leads to the conclusion that the emission arises from thin sheets of hot gas. Hollenbach and Shull (1977) originally suggested this region as a possible source of H_2 emission due to shock heating induced by a stellar wind.

I evaluated the possibility of NUV excitation in LkHα 349 as I did for the H_2 emission near HII. In this case the calculations were made using the central star of IC 1396 (BD +56 2617) and again they indicate that NUV fluorescence is unlikely to be responsible for the observed H_2 emission. In the absence of any indication of a hidden early type star near LkHα 349 I did not consider the possibility of NUV excitation from within the cloud. This would, of course, greatly reduce the luminosity requirements on the exciting star. LkHα 349 itself was not considered as a possible NUV source since its apparent temperature is too low and no indirect indication of a strong UV flux, such as a compact radio continuum source, is known to be present.

The H_2 source near LkHα 349 may represent a type of H_2 emission region distinct from the Orion, S140, W3(OH), NGC 7538 group. Although LkHα 349 is located in a dense cloud, it is a small, isolated cloud with no known compact IR sources, masers or radio continuum sources and,

while LkHα 349 itself may be a young object, the region is not obviously a site of active star formation. LkHα 349 is an emission line star of spectral type F6 to F8 (Dibai, 1969), an object uncharacteristic of the H_2 emission regions of the Orion group of H_2 sources. Loren, Peters and Vanden Bout discuss the possibility that LkHα 349 is similar to Herbig Be and Ae stars, all of which are associated with CO molecular clouds. In view of this possible association, searches for H_2 emission from the CO clouds of known Be and Ae stars might prove fruitful.

Planetary Nebulae

H_2 emission from planetary nebulae was first reported from NGC 7027 by Treffers et al. (1976). Beckwith, Persson and Gatley (1978) undertook a survey of several planetary nebulae for 2 μ H_2 emission, confirming the H_2 emission from NGC 7027 as well as detecting emission from five other nebulae. Our survey measurement of 7027 used a much larger beam size than previously reported observations and consequently gives information on the angular extent of the H_2 emission. Our measurement of the S(1) flux from 7027 with a 36" beam is about twice that indicated by Beckwith, Persson and Gatley, who used a beam presumably about three times smaller. This result and private discussions with R. Treffers (1978), who has observed S(1) in 7027 with a 60" beam, indicate that, while there is a central concentration of the H_2 emission from 7027, a sizable fraction, perhaps one half, may come from a region 36" in diameter outside of the central core.

All other planetary nebulae included in our survey show no detectable H_2 emission and so extend Beckwith, Persson, and Gatley's

list of non-emitting planetaries. IC 418 is notable in that it, like 7027, is one of the planetary nebulae in which Mufson, Lyon and Marionni (1975) detected CO emission. The absence of H_2 emission from IC 418 at a level of about half the flux from 7027 indicates that a molecular cloud near a planetary nebula is not a sufficient condition for H_2 emission. Beckwith, Persson and Gatley have already shown that nearby molecular clouds are not a necessary condition for H_2 emission from planetary nebulae.

It is a priori somewhat surprising to find molecular hydrogen emission from a high excitation object such as a planetary nebula which is not near a dense concentration of interstellar material such as a molecular cloud. Black (1978), however, has predicted significant column densities of several molecular species, including H_2, to be present in the transition zone from HII to HI of planetary nebulae. A spatially resolved study of the H_2 1-0 S(1) emission from NGC 6720, the Ring Nebula, by Beckwith, Persson and Gatley (1978) revealed that the H_2 emission was associated with the [OI](λ6300) emission. [OI] emission is produced in the transition zone or in the filaments or clumps of material which are optically thick to Lyman continuum radiation. The correlation of H_2 with [OI] probably indicates that H_2 lies within the transition zone as predicted by Black and makes the presence of H_2 emission from planetary nebulae a more understandable phenomenon. The excitation mechanism of the H_2 in planetary nebulae is as yet unknown. The probable operation of the ultra-violet fluorescence mechanism, the most likely possibility according to Black (1978), would be easily

detectable by the presence of the 2-1 S(1) line at a strength a little more than one half that of the 1-0 S(1) line. Shock heating models predict a 2-1 S(1) to 1-0 S(1) ratio of <0.2 in regions where the conditions are proper for shock heating.

External Galaxies and Our Galactic Center

The 1-0 S(1) and S(2) lines of H_2 have been detected in the spectrum of NGC 1068 by Thompson, Lebofsky and Rieke (1978) using the Steward Observatory fourier transform spectrometer (Thompson and Reed, 1975). They find that the relative strengths of the 1-0 S(1) and S(2) lines are similar to those in the Orion H_2 source and that, like Orion and unlike the Black and Dalgarno NUV fluorescence mechanism, the 2-1 S(1) is absent and therefore conclude that the H_2 in 1068 is probably shock heated. Under this assumption the S(1) and S(2) ratio indicates a temperature of between 800K and 3400K which is at least consistent with the theroetical shock heating range of 1600K to 2000K.

We examined the Seyfert galaxy NGC 4151 for H_2 emission very early in the survey program. No H_2 emission was detected but the upper limit set is not as low as the level of emission from NGC 1068. Neither was any H_2 emission seen from NGC 5195, the companion to M51, anywhere along a 36" wide scan through the galaxy's center along its major axis. NGC 5236 also showed no detectable H_2 emission.

Our observations of Sgr A show no H_2 emission down to a rather low level in a 36" circular area around IRS-7 as compared to immediately adjacent 36" areas to the east and west. This observation does not eliminate the possibility of substantial amounts of excited

molecular hydrogen in the center of the Galaxy since a considerable amount of extinction of 2 μ radiation may occur between the sun and the Galactic center. This observing method also would not detect an H_2 emission region larger than 100" centered at the Galactic center.

T Tauri

Beckwith, Gatley, Matthews, and Neugebauer (1978) have detected the 1-0 S(1) line of H_2 from a region $\tilde{>}$ 5" in size around T Tauri. The 2-1 S(1) line was not detected. Four other T Tauri stars were examined by Beckwith et al. but none showed detectable H_2 emission. We observed T Tauri and found an indication of 1-0 S(1) but were not able to get enough observations to push our signal to noise ratio far enough for a confirmed detection.

Supernova Remnants

None of the SNR's observed in the survey showed a statistically significant level of H_2 emission. SN+1604 (3C358, Kepler's SNR) did show an indication of H_2 3'20" to the west of the position of the nova (Baade, 1943). Since only one set of measurements was made of this area and the H_2 indication was only barely at a significant level, SN+1604 is listed in table 4 as a possible source only. SN+1572 and M1 also showed some positive indications for H_2 which I was not able to confirm or eliminate. Unfortunately, the R association CMa R1, which has been the object of considerable study in connection with supernova induced star formation (Herbst and Assousa, 1977), was not included in

the survey. This association should be an interesting candidate for molecular hydrogen emission.

CHAPTER 8

SUMMARY

In the course of a previous dissertation project, emission from several lines in the 1-0 band of the molecular hydrogen quadrupole spectrum was discovered in 2 μ spectra of a part of the Orion nebula. Our analysis of these lines revealed that the emitting H_2 was probably not excited by ultra-violet radiation from nearby hot stars but rather was thermally excited to a temperature near 2000K. Using our derived column density and the requirement of a minimum space density of H_2 to produce thermal excitation, other authors deduced that the excited H_2 occurred in thin sheets. We had suggested that the hot H_2 could be produced by shock waves and subsequent theoretical work by several groups indicated that shock heating would produce the radiation we observed under the conditions expected in the Orion molecular cloud. It remains, however, difficult to find an energy source adequate to drive the required shock in the Orion cloud.

The relative ease of detection of the Orion H_2 lines and the additional detection of H_2 emission from NGC 7027 offered the possibility that the 2 μ molecular hydrogen lines could not only be used to probe deep into heavily obscured regions of interstellar space but could also provide new information on a variety of different astronomical objects. With this in mind we began the construction of a new instrument optimized to search for new molecular hydrogen emission.

We developed a tilting filter monochromator, a technique previously unused in infra-red astronomy, into a sensitive, efficient instrument for astronomical observations. We have shown that such an efficient, wide field monochromator of moderate resolution is an effective instrument with which to search for 2 μ emission from interstellar molecular hydrogen.

The survey for new H_2 emission using the tilting filter spectrometer resulted in the discovery of four new H_2 sources. The Sharpless 140, W3(OH) and NGC 7538 (N)-OH molecular hydrogen sources lie in large, dense molecular clouds near sites of active star formation. The LkHα 349 source lies in a small, isolated molecular cloud where star formation is not obviously active and may represent a class of H_2 emission object separate from the other new sources.

Analysis of these new sources in terms of recent theoretical investigations of ultra-violet fluorescence and shock heating in molecular hydrogen indicates that ultra-violet excitation of the H_2 is not an attractive explanation for the emission but that the physical condition of the H_2 in the new sources is compatible with the requirements of shock heating. If shock heating is assumed to excite the new sources, the excited molecular hydrogen is probably confined to thin sheets as it appears to be in the Orion source.

The work described in this dissertation and the efforts of several other investigators have now produced a sizable list of objects which show 2 μ molecular hydrogen emission. H_2 emission objects now include active regions of large molecular clouds, planetary nebulae,

T Tauri stars, Seyfert galaxies and one small, isolated molecular cloud near an emission line star. These results have been achieved in spite of the fact that all molecular hydrogen sources discovered since Orion have had brightnesses near the detection limit of existing instrumentation. However, recent advances in the application of indium antimonide detectors through the use of helium cooling will allow an increase in sensitivity by a factor of three to five which should put many more H_2 emission regions within the reach of new instrumentation. Future studies of 2 μ emission from interstellar molecular hydrogen promise to provide exciting and useful new information on a wide variety of astronomical objects.

REFERENCES

Baade, W., 1943, Ap. J., 97, 119.

Beckwith, S., Gatley, I., Matthews, K., and Neugebauer, G., 1978, Ap. J. Letters, 223, L41.

Becklin, E. E., and Neugebauer, G., 1968, Interstellar Ionized Hydrogen, p. 5, ed. Y. Terzian (New York: Benjamin).

Beckwith, S., Persson, S. E., and Gatley, I., 1978, Ap. J. Letters, 219, L33.

Beckwith, S., Persson, S. E., Neugebauer, G., and Becklin, E. E., 1978, Ap. J., 223, 464.

Black, J. H., 1978, Ap. J., 222, 125.

Black, J. H., and Dalgarno, A., 1976, Ap. J., 203, 132.

Blair, G. N., Evans, N. J., Vanden Bout, P. A., and Peters, W. L., 1978, Ap. J., 219, 896.

Carruthers, G. R., 1970, Ap. J. Letters, 161, L81.

Dibai, E. A., 1969, Astrofizika, 5, 249.

Dibai, E. A., and Esipov, V. F., 1968, Sov. Astr. AJ, 12, 448.

Eather, R. H., and Reasoner, D. L., 1969, Appl. Optics, 8, 227.

Field, G. B., Rather, J. D. G., Aannestad, P. A., and Orzag, S. A., 1968, Ap. J., 151, 953.

Field, G. B., Somerville, W. B., and Dressler, K., 1966, Ann. Rev. Astron. & Astrophys., 4, 207.

Fink, U., 1965, Ph. D. Dissertation, Pennsylvania State University, Department of Physics.

Fink, U., Wiggins, T. A., and Rank, D. H., 1965, J. Mol. Spectrosc., 18, 384.

Gatley, I., Becklin, E. E., Matthews, K., Neugebauer, G., Penston, M. V., and Scoville, N., 1974, Ap. J. Letters, 191, L121.

Gautier, T. N., Fink, U., Treffers, R. R., and Larson, H. P., 1976, Ap. J. Letters, 207, L129.

Gillett, F. C., and Forrest, W. J., 1973, Ap. J., 179, 483.

Gould, R. J., 1964, Ap. J., 140, 638.

Gould, R. J., and Harwit, M., 1963, Ap. J., 137, 694.

Grasdalen, G. L., 1976, Ap. J. Letters, 205, L83.

Gull, T. R., and Harwit, M. O., 1971, Ap. J., 168, 15.

Hall, D. N. B., Aitkins, R. S., Joyce, R., and McCurnin, T. W., 1975, Appl. Optics, 14, 450.

Hall, D. N. B., Hinkle, K., Ridgway, S. T., and Wojslaw, R., unpublished paper, Kitt Peak National Observatory, Tucson, Arizona.

Hall, D. N. B., Kleinmann, S. G., Ridgway, S. T., and Gillett, F. C., 1978, Ap. J. Letters, 223, L47.

Harvey, P. M., Campbell, M. E., and Hoffmann, W. F., 1978, Ap. J., 219, 891.

Herbst, W., and Assousa, G. E., 1977, Ap. J., 217, 473.

Hollenbach, D. J., and Shull, J. M., 1977, Ap. J., 216, 419.

Joyce, R. R., Gezari, D. Y., Scoville, N. Z., and Furenlid, I., 1978, Ap. J. Letters, 219, L29.

Joyce, R. R., and Grasdalen, G. L., 1976, Bull. AAS, 8, 349.

Joyce, R. R., Simon, M., and Simon, T., 1978, Ap. J., 220, 156.

Knapp, G. R., Brown, R. L., Kuiper, T. B. H., and Kakar, R. K., 1976, Ap. J., 204, 781.

Kwan, J., 1977, Ap. J., 216, 713.

Kwan, J., and Scoville, N., 1976, Ap. J. Letters, 210, L39.

Lada, C. J., and Black, J. H., 1976, Ap. J. Letters, 203, L75.

Lada, C., Dickinson, D. F., and Penfield, H., 1974, Ap. J. Letters, 189, L35.

Lambert, D. L., Brooke, A. L., and Barnes, T. G., 1973, Ap. J., 186, 573.

Larson, H. P., and Fink, U., 1975, Appl. Optics, 14, 2085.

Lemke, D., and Low, F. J., 1972, Ap. J. Letters, 177, L53.

Liszt, H. S., Wilson, R. W., Penzias, A. A., Jefferts, K. B., Wannier, P. G., and Solomon, P. M., 1974, Ap. J., 190, 557.

London, R., McCray, R., and Chu, S. I., 1977, Ap. J., 217, 442.

Loren, R. B., Peters, W. L., and Vanden Bout, P. A., 1975, Ap. J., 195, 75.

Martin, A. H. M., 1973, MNRAS, 163, 141.

Martin, A. H. M., and Downes, D., 1972, Astrophys. Letters, 11, 219.

Mezger, P. G., Altenhoff, W., Schraml, J., Burke, B. F., Reifenstein, E. C., and Wilson, T. L., 1967, Ap. J. Letters, 150, L157.

Minkowski, R., 1968, Nebulae and Interstellar Matter, p. 623, ed. Middlehurst, B. M. and Aller, L. H., (Chicago: University of Chicago Press).

Mufson, S. L., Lyon, J., and Marionni, P. A., 1975, Ap. J. Letters, 201, L85.

Ogden, P. M., Roesler, F. L., Reynolds, R. J., Scherb, F., Larson, H. P., Smith, H. A., and Daehler, M., 1978, unpublished paper, Department of Physics, University of Wisconsin, Madison, Wisconsin.

Osterbrock, D., 1962, Ap. J., 136, 359.

Panagia, N., 1973, AJ, 78, 929.

Prentiss, A. J. R., and ter Haar, D., 1969, MNRAS, 146, 423.

Rubin, R. H., 1968, Ap. J., 154, 391.

Ryle, M., Elsmore, B., and Neville, A. C., 1965, Nature, 205, 1259.

Shull, J. M., 1978, Ap. J., 219, 877.

Shull, J. M., and Hollenbach, D. J., 1978, Ap. J., 220, 525.

Spinrad, H., 1964, Ap. J., 140, 1639.

Spinrad, H., 1966, Ap. J., 145, 195.

Spinrad, H., and Wing, R. F., 1969, Ann. Rev. Astron. & Astrophys., 7, 249.

Spitzer, L., Drake, J. F., Jenkins, E. B., Morton, D. C., Rogerson, J. B., York, D. G., 1973, Ap. J. Letters, 181, L116.

Strom, R. G., and Duin, R. M., 1973, Astron. and Astrophys., 25, 351.

Thompson, R. I., Lebofsky, M. J., and Rieke, G. H., 1978, Ap. J. Letters, 222, L49.

Thompson, R. I., and Reed, M. A., 1975, Pub. ASP, 87, 929.

Treffers, R. R., 1978, Private communication. Research Associate in Astronomy, University of California, Berkeley, California.

Treffers, R. R., Fink, U., Larson, H. P., and Gautier, T. N., 1976, Ap. J., 209, 793.

Werner, M., 1968, Ph. D. Dissertation, Cornell University, CRSR Report N. 316.

Werner, M. W., and Harwit, M., 1968, Ap. J., 154, 881.

Wynn-Williams, C. G., 1971, MNRAS, 151, 397.

Wynn-Williams, C. G., Becklin, E. E., and Neugebauer, G., 1972, MNRAS, 160, 1.

Wynn-Williams, C. G., Becklin, E. E., and Neugebauer, G., 1974, Ap. J., 187, 473.